JOURNAL OF GEOPHYSICAL RESEARCH, VOL. 112, B03213, doi:10.1029/2006JB004445, 2007

Using the Level-Set Method to Model Endogenous Lava Dome Growth.

A. J. Hale, L. Bourgouin and H. B. Mühlhaus

Earth Systems Science Computational Centre (ESSCC),

Australian Computational Earth Systems Simulator (ACcESS),

The University of Queensland, Australia

Tel: +61 7 3346 4110, Fax: +61 7 3346 4134, e-mail: alinah@esscc.uq.edu.au

Received 12 April 2006; accepted 21 November 2006; published 31 March 2007.

Keywords: lava flow; level set method; computational volcanology.

Index Terms: 8414 Volcanology: Eruption mechanisms and flow emplacement; 0545 Computational Geophysics: Modeling (4255); 8425 Volcanology: Effusive volcanism.

Abstract

Modeling volcanic phenomena is complicated by free-surfaces often supporting large rheological gradients. Analytical solutions and analogue models provide explanations for fundamental characteristics of lava flows. But more sophisticated models are needed, incorporating improved physics and rheology to capture realistic events. To advance our understanding of the flow dynamics of highly viscous lava in Peléean lava dome formation, axi-symmetrical Finite Element Method (FEM) models of generic endogenous dome growth have been developed. We use a novel technique, the level-set method, which tracks a moving interface, leaving the mesh unaltered. The model equations are formulated in an Eulerian framework. In this paper we test the quality of this technique in our numerical scheme by considering existing analytical and experimental models of lava dome growth which assume a constant Newtonian viscosity. We then compare our model against analytical solutions for real lava domes extruded on Soufrière, St. Vincent, W.I. in 1979 and Mount St. Helens, USA in October 1980 using an effective viscosity. The level-set method is found to be computationally light and robust enough to model the free-surface of a growing lava dome. Also, by modeling the extruded lava with a constant pressure head this naturally results in a drop in extrusion rate with increasing dome height, which can explain lava dome growth observables more appropriately than when using a fixed extrusion rate. From the modeling point of view, the level-set method will ultimately provide an opportunity to capture more of the physics while benefiting from the numerical robustness of regular grids.

1. Introduction

Lava domes are steep-sided mounds of lava formed from slowly extruded silicic magma. They form during an eruption when the extruded lava is so viscous that it can't flow freely away from the vent and a lava dome may consist of one or more individual lava lobes. Their propensity to collapse in a hazardous manner [*Voight,* 2000] makes them of concern to the surrounding area. Progress still needs to be made to enable us to learn more about the mechanics of growing lava domes despite recent advances in experimental [*Griffiths and Fink,* 1993] and theoretical modeling [*Balmforth et al.,* 2001]. This requires the formulation of physically consistent models, the incorporation of experimental research to improve our understanding of the rheology as well as the development of more effective numerical techniques for the simulation of realistic events. This paper focuses upon this last point.

What makes modeling lava domes/flows so complicated is that they can take numerous growth styles and display a range of morphological features that partly reflect the highly variable nature of the lava rheology, the shape of the surrounding ground and the earlier erupted lava masses. Lava domes generally spread laterally and inflate vertically via the addition of new lava within the body of the dome representing a thermo-mechanical continuum in their early stages of growth, which is known as endogenous dome growth. However, this regime is often interrupted via the formation of an internal discontinuity (a fault or shear band) which results in lava being extruded directly to the free surface, a regime known as exogenous growth. The models discussed here focus upon endogenous dome growth, being the simplest growth form, most frequently modeled and best understood to date.

Current models provide us with qualitatively consistent observations as well as providing some quantitative insight into the eruption dynamics. Advances into the material rheology of lava have lead to *Melnik and Sparks* [1999] demonstrating that multiple steady state solutions can exist for fixed system parameters for conduit flows related to dome extrusion rates. This is attributed to relative time scales of magma ascent and crystallization induced by gas exsolution [*Melnik and Sparks*, 2005]. Unfortunately these models do not allow the simulation of free-surfaces. *Iverson* [1990] recognition of the importance of a chilled carapace or skin with different properties to those of the interior of the dome led to this feature being incorporated into analytical models. Modeling the free surface of a lava flow is of primary importance because it's where the largest rheological changes occur, but previous numerical work has shown this to be a challenging enterprise [*Hale and Wadge*, 2003]. In this paper we present a novel technique to model simple endogenous lava dome growth by tracing the free-surface without altering the model space/mesh. In this way the benefits of a regular (e.g. rectangular) mesh are retained yet domain boundaries can be accounted for in a relatively non-diffusive way [*Sussman et al.*, 1994]. Previous FEM volcanological models based on an arbitrary Lagrangian-Eulerian scheme have required mesh updates and frequent re-meshing (due to element distortion) which is time-consuming and results in a loss of accuracy because of the need to interpolate data between the integration points of the integration scheme [*Hale and Wadge*, 2003]. Re-meshing can also result in a loss of information due to the difficulty of extracting information and re-entering this information into a different model domain. Time-dependent processes can easily be modeled using the level-set method due to the retention of information within the model domain. History dependence in the model will allow for consideration of out-of-equilibrium processes such as crystal growth which opens up new and advanced modeling opportunities.

In this paper we test the capability of the level-set method against existing analytical and experimental models of lava dome growth which assume a constant Newtonian viscosity. This necessary simplification makes the calculations tractable for comparison to existing models. Using a Newtonian viscosity also enables us to understand the fundamental first-order processes associated with simple dome growth before attempting more complex rheological effects. This issue is discussed further at the beginning of the next section. We discuss the computational technique used in the model and describe its parameterization. We compare our model to *Huppert et al.'s* [1982] analytical study and *Buisson and Merle's* [2002, 2004] experimental research. We then use data from the lava domes emplaced on Soufriere, St. Vincent, W.I. in 1979 and Mount St. Helens, USA in October 1980, to model lava dome growth for a variable extrusion rate and for a constant pressure head using an effective viscosity for the lava.

2. Model Development

Our modeled lava dome grows onto a horizontal base fed by lava from a conduit at a mass flux rate Q, or constant pressure P. The lava is modeled as a Newtonian fluid with a constant viscosity in an axisymmetrical coordinate system. Real lava exhibits strong temperature dependence, which in connection with dome growth manifests itself by a thin, highly viscous (in fact: elasto-visco-plastic) crust at the surface of the dome. To resolve this effect computationally would require dynamic re-meshing (mesh refinement) around the dome surface. The situation is not unlike the situation in mantle convection with temperature dependent viscosity. Dynamic re-meshing is computationally expensive and we are currently working on an equivalent shell model attached to the level set function. Here a constant viscosity is assumed because the main purpose

of this paper is to test the quality of the approximation of our numerical scheme (described below) against analytical and semi analytical solutions all of which assume a constant viscosity.

The axisymmetrical model domain for the initial and a later time step are shown in Figure 1 with the domain rotated about r=0. The lower right part of the model domain is the surface of the volcano and here the velocity is set to zero, **v** = (0,0). The boundary condition at the conduit inlet, i.e. the path to the magma chamber, is described by a stress boundary condition in the form $\sigma_{zz} = -P^0$ (constant pressure head) as shown in Figure 1 with zero shear stress; alternatively we assume a parabolic velocity distribution $v_z = v_0(1-(r/a)^2)$, where a is the conduit radius (see Figure 1). The corresponding extrusion rate of dimension volume per unit time is obtained as $Q = \frac{1}{2}\pi a^2 v_0$. Both lava and the surrounding embedding-medium ("air") are modeled as constant viscosity fluids and the volcano surface on which the lava dome spreads is assumed as rigid. The internal boundary conditions (stress traction and velocity continuity) at the lava/embedding-medium interface are automatically satisfied since the domain occupied by the embedding medium is part of the model. Zero stress tractions are assumed at z=H and at r=R for z>h. As in the papers by *Huppert et al.* [1982] and *Buisson and Merle* [2002, 2004] temperature effects are not considered in this paper. The influence of heat flow in the surrounding embedding-medium and volcano surface as well as the effect of the volcano surface deformation on the dome morphology will be explored in a forthcoming paper. After each velocity time-step the interface between the lava and the embedding-medium is advected into the model domain as shown for t=tn (Figure 1). A major advantage of this model over previous FEM models is that the lava dome can effectively be grown from nothing. Previous FEM lava dome models [*Hale and Wadge*, 2003] have required an initial free-surface condition for the lava dome surface which can

affect the final results, whilst this model only requires an initial height level of lava in the conduit.

We define the Reynolds number as $\mathrm{Re} = \rho_{lava} VL / \eta_{lava}$, where ρ_{lava}, V and L are the density of the lava, characteristic velocity and characteristic length respectively. We define V either as $V = Q/(\pi a^2)$ if Q is given or as the average velocity of a Hagen-Poiseulle flow in the conduit with a pressure gradient of P^0 / h for the constant pressure head boundary condition model. In the latter case we obtain $V = a^2 h/(8\eta_{lava} P^0)$. Assuming L=h we obtain values for Re in the order 10^{-11}; hence inertia effects can be safely neglected. In other words, for the present problem the lava and the surrounding medium flow are governed by the axi-symmetric Stokes equations (see equation A4 in the Appendix). Beside the Newtonian constitutive relationship for the deviatoric stresses, we assume the following relationship for the pressure rates:

$$p_{,t} = -K_\alpha div\mathbf{v} \qquad (1)$$

Where K_α is the elastic bulk modulus of lava ($\alpha = 1$) or embedding medium ($\alpha = 2$) respectively at a given reference pressure and temperature, the index comma followed by the index t denotes the partial derivative with respect to time. The material time derivative of the pressure was replaced by the partial time derivative for simplicity and this approximation is admissible for weakly compressible media [e.g. *Zienkiewicz & Taylor,* 2000, p. 6&11]. During time integration of our model equations, the partial time derivative in (1) is replaced by the difference expression $(p^{t+\Delta t} - p^t)/\Delta t$. This method is sensitive to the choice of the initial

pressure. In the present study we assume an initial lithostatic pressure distribution in the conduit. The governing equations (A4) are non-dimensionalized using the length and time scales a and $\pi a^2 h/Q$ (Figure 1), where Q is a measure for the flux at the base of the conduit. In the case of the prescribed flux boundary condition Q is given; for the constant pressure head boundary condition we define Q as $Q = \pi a^2 P^0 h/\eta_{lava}$, this results in equations A7. By inspection of the coefficients in A7 we notice that the flow is effectively incompressible when $\pi a^2 h K_\alpha /(Q\eta_\alpha \Delta\tilde{t}) >> 1$, where $\Delta\tilde{t}$ is the non-dimensional time increment. During the simulation the time increment is determined in each time step from a Courant condition [*Zienkiewicz and Taylor*, 2000, p. 42] assuming a Courant number of 0.3. For realistic values of K and P^0 it turns out that $\pi a^2 h K_\alpha /(Q\eta_\alpha \Delta\tilde{t})$ is so large that we decided to replace $\pi a^2 h K_\alpha /(Q\eta_\alpha \Delta\tilde{t})$ by a constant penalty factor in conjunction with reduced order shape functions for the pressure to avoid numerical instabilities [*Zienkiewicz and Taylor*, 2000, Vol. 1].

2.1 Level-set method

In computational volcanology, a jump in the fluid characteristics, viscosity and density, exists across the interface between the embedding-medium and the lava, and the evolution of the system strongly depends on the fluid-to-fluid interaction. Therefore, accurate calculation of the interface evolution is critical for the problem solution. Level set methods, introduced by *Osher and Sethian* [1988], are computational techniques for tracking moving interfaces. They rely on an implicit representation of the interface whose equation of motion is numerically approximated using schemes built from those for hyperbolic-conservation laws. Level set methods are particularly designed for problems in multiple dimensions in which the topology of the evolving interface

changes during the course of events and for problems in which sharp corners and cusps are present.

A scalar function ϕ is initialized over the domain as a "signed" distance function with respect to the interface with a gradient of unity. The interface is represented as the zero level-set of this function. At each time step, once the velocity v is solved, the new ϕ is calculated by solving the advection equation:

$$\phi_{,t} + v \cdot \nabla \phi = 0 \tag{2}$$

Special care must be taken when solving the advection equation to avoid numerical diffusion. Various upwinding schemes exist to achieve this goal, such as the streamline upwind Petrov-Galerkin (SUPG) formulation. The most efficient scheme found by the authors is the Taylor-Galerkin formulation [*Zienkiewicz and Taylor,* 2000, p. 47]:

$$\phi^{+} = \phi^{-} - \Delta t \left(v \cdot \nabla \phi^{-} \right) + \frac{\Delta t^2}{2} v \cdot \nabla \left(v \cdot \nabla \phi^{-} \right) \tag{3}$$

The property of ϕ being a distance function is not preserved in general during advection due to the variation in the viscosity field over the model domain. It has however been shown by *Sussman et al.* [1994], that it is critical that ϕ remains a distance function in regions close to any interface, in order to obtain acceptable conservation of mass. Therefore, a reinitialization procedure is required. The following equation was introduced by *Sussman et al.* [1994]:

$$\psi_{,\tau} = sign(\phi)(1-|\nabla\psi_0|)\,, \tag{4}$$

where τ is an artificial time. Solving the above equation to a steady state and using $\psi_0 = \phi$, the solution will have the same zero level set as ϕ and will be a real distance function ($|\nabla\psi| = 1$). This equation can also be written as:

$$\psi_{,\tau} + w\cdot\nabla\psi = sign(\phi) \qquad \text{with} \qquad w = sign(\phi)\frac{\nabla\psi}{|\nabla\psi|} \tag{5}$$

A Taylor Galerkin procedure is again used, the reinitialization consists in solving:

$$\psi^{+} = sign(\phi) + \psi^{-} - \Delta t\left(w\cdot\nabla\psi^{-}\right) + \frac{\Delta t^2}{2} w\cdot\nabla\left(w\cdot\nabla\psi^{-}\right) \tag{6}$$

In practice, there is no need to solve this equation to steady state over the entire domain as only the nodes closest to the interface are of interest for the method. Consequently, the stopping criterion for the reinitialization equation is considered only on a narrow band around the interface. The bandwidth is chosen equal to six times the size of an element. Moreover, the reinitialization only needs to be done only when ϕ gets too distorted. In practice ϕ is reinitialized every five time steps. To demonstrate the importance of reinitializing, Figure 2 shows five isosurfaces of ϕ around the zero level set after four hundreds time steps. It can be

clearly seen that without reinitialization ϕ is no longer a smooth distance function. This introduces error on the calculation of the position of the interface later in the simulation.

When the new distance function is found, the physical parameters are updated using, for a given parameter P:

$$P = \begin{cases} P_1 & where \psi < -\alpha h \\ P_2 & where\ \psi > \alpha h \\ \dfrac{P_2 - P_1}{2\alpha h}\psi + \dfrac{P_1 + P_2}{2} & where\ |\psi| < \alpha h \end{cases} \quad (7)$$

where h is the size of the elements in the mesh and α is a smoothing parameter. This has the effect of smoothing the physical parameters across the interface, on a band of width $2\alpha h$. In this paper α is taken equal to 1. The smoothing procedure prevents numerical instabilities when solving the stress equilibrium.

The algorithm can be summarized as follow:

1. Initialize ϕ as a signed distance function to the interface
2. Update the parameters on the mesh
3. Solve the stress equilibrium to get the velocity v
4. Solve the advection equation using v to get the new ϕ
5. Reinitialize ϕ if necessary to get ψ
6. End of time step, repeat 2 to 5

Currently our models consider a difference in viscosity between the lava and embedding-medium of an order of magnitude, with the embedding medium having the lower viscosity. Models have been solved with a larger viscosity difference, up to three orders of magnitude, but they are numerically less stable. However it is observed that there is very little difference in the free-surface shape for viscosity differences between the lava and embedding-medium greater than an order of magnitude over the time-scales we consider. For example, after 4000 time-steps (a model time period of 16 days) the difference in maximum height for a model with a viscosity contrast of one order or magnitude against a viscosity contrast of two orders of magnitude was less than the node spacing as used in our models. Because the model contains a compressibility term (the inverse of the bulk modulus) it is expected that the modeled lava will experience some degree of volume loss over time. It is found that this volume loss is small, an approximately 3% difference in the values obtained for the modeled volume against the theoretically calculated volume as shown in Figure 3. The initial height of the interface is set to be several elements below the surface of the volcano. This prevents the advected level-set zero values merging with the stationary level-set zero values within the surface domain (Figure 1). This results in a delay before the height of the lava in the shallow conduit reaches the surface of the volcano.

3. Results

Our computational model is tested against four case studies. First we consider the analytical study for a spreading Newtonian lava dome with a constant extrusion rate presented by *Huppert et al.* [1982]. Following this we consider experimental research by *Buisson and Merle* [2002, 2004] for an understanding of the free-surface shape and the strain-rate field within the dome. We

263 then apply our model to the lava dome extruded on Soufrière St Vincent, W.I. in 1979 using the
264 method presented by *Huppert et al.* [1982] and for a constant applied pressure-head. Finally we
265 consider the lava dome extruded on Mount St. Helens, USA in October 1980. Both of these real
266 lava domes are particularly suitable as test cases because they were both extruded approximately
267 axisymmetrically suggesting endogenous growth, they grew on approximately flat unconstrained
268 surfaces and most importantly data exists for their evolution over time.
269

270 **3.1 Comparison to Huppert et al.'s model**

271 *Huppert et al.* [1982] consider a theoretical treatment for a Newtonian fluid with constant
272 kinematic viscosity ν spreading on a horizontal surface. The Reynolds number, as for lava flows,
273 is assumed to be small enough such that inertial effects can be neglected. They model the
274 spreading fluid as a balance between the driving force from the hydrostatic pressure and the
275 viscous retarding force and find that for a constant extrusion rate the maximum radial extent of
276 the flow r_N can be described by:
277

278 $$r_N = 0.715\left(gQ^3/3\nu\right)^{1/8} t^{1/2} \quad (8)$$

279

280 where g is the acceleration due to gravity, Q is a constant extrusion rate and t is time. To test the
281 validity of this model *Huppert et al.* [1982] carried out a series of laboratory experiments using a
282 Newtonian viscous fluid. Here we test our model results against their theoretical analysis. Table 1
283 lists the conditions of each of our model runs with all runs using a density of 2400 kgm^{-3} and

Figures 4 and 5 show our results normalized by $\left(gQ^3/3\nu\right)^{1/8}$ against the theoretical result obtained by *Huppert et al.* [1982].

Figures 4 and 5 show that our results follow the same trend as *Huppert et al.'s* [1982] theoretical curve at later times in the evolution of the dome, but in the early stages of dome growth there is an initial departure from this curve. There are several processes creating the departure from the theoretically predicted trend at early times in the dome evolution. First our calculated radius can not be smaller than the modeled conduit radius and thus an initial time at r=0 can not be assumed. In our model we use a finite conduit radius of 15 meters. *Huppert et al.'s* [1982] model assumes an infinitesimally small conduit and all the fluid enters the dome at r=0. This is unphysical and results in a singularity in their analysis at r=0. Therefore by modeling dome growth with a finite radius as in our model we can only apply *Huppert et al.'s* [1982] analysis when the lava dome has spread beyond the conduit radius. Secondly there is a short time-delay for the lava to move up the conduit in the model and to reach the conduit exit because the initial height level of the lava is modeled to be 5 meters below the conduit exit. Finally the extruding lava will have vertical momentum attained from the conduit inlet boundary condition which results in a central uplift area and initially limits lateral spreading. At later times in the dome growth, when the lava dome radius is much larger than the conduit radius, and the height of the dome has reached its asymptotic limit, these effects can be ignored and the dome radius grows as proportional to the square-root of time, as calculated by *Huppert et al.* [1982] following a mass conservation law. This initial departure in our modeled normalized radius from the theoretical solution derived by *Huppert et al.* [1982] is considered in more detail in section 4.2 after *Buisson and Merle's* [2002, 2004] research has been discussed.

Our models also allow the extraction of information regarding the height and free-surface of the lava dome over time and we will consider the lava dome structure in more detail in the next section.

3.2 Lava dome structure

Analogue models are often used in volcanological research to capture generic processes and surface morphology [*Griffiths,* 2000]. Unfortunately there is no single analogue model that can replicate all the known processes in lava and it is difficult to model a large parameter space. This is where computational models have the advantage. Here we compare our computational model of generic endogenous dome growth to experimental simulations of the strain field within analogue lava domes performed by *Buisson and Merle's* [2002, 2004]. Their 2002 paper considers simple dome analogue models to investigate the internal stress and strain field evolution in an endogenous lava dome by modeling the lava as a very viscous fluid. For this they use silicon gel, which behaves in a Newtonian fashion over their time-scales considered. They inject the gel vertically from a reservoir into a feeding conduit and onto a rigid horizontal plane for three-dimensional models and our computational models replicate this experimental set-up. Whilst for two-dimensional models *Buisson and Merle* [2002] inject the silicon gel between two lubricated glass walls. The extrusion rate was kept constant for all their models and they also recorded information about the height, radius and free-surface.

3.2.1. Analysis of Dome Flow Structure

Buisson and Merle's [2002] two-dimensional glass confined models make it possible to observe the internal strain field by tracing particle paths or observing the deformation of a carbon grid imprinted onto the fluid. In vertical cross-section particle trajectories are observed to be parabolic and symmetric about the feeding conduit and they observe two types of particle path. Particles extruded from the lateral sides of the feeding conduit show an initial rising within the dome which subsequently becomes horizontal or even downwards as the particle moves towards the dome margin. Particles extruded from the central part of the feeding conduit exhibit initial strong vertical rising which is due to the injection force locally overcoming gravity. These competing effects split the dome into two flow domains: a central region of the dome experiencing uplift from the injection force and a region away from this which deforms purely due to gravity. This split in flow domains was also observed in our models and a cartoon of this effect is shown in Figure 6.

To evaluate if our model captures the flow effects experienced in a real Newtonian fluid we extract the free surface information from our computational model. The free-surface profile in time for two model runs are shown in Figures 7a and b for half a lava dome rotated about where the radius equals zero. The modeled lava has a viscosity of $2x10^9$ Pa s and in Figure 7a the extrusion rate is $17.5m^3s^{-1}$, whilst in Figure 7b it is $0.175m^3s^{-1}$. The time-difference between each surface corresponds to approximately 100 minutes and 52 hours for Figures 7a and 7b respectively. The main difference between these model runs is the relative time for the lava to deform via gravity and vertical injection. Figure 7a shows that initially dome growth is predominantly vertical due to a high extrusion rate; however as the height growth-rate slows the lava spreads laterally. Due to the injection force the surface of the dome bulges in the centre and

352 becomes flatter towards the edges. This central region as well as bulging of the dome laterally, is
353 more pronounced in Figure 7a than in 7b due to a higher extrusion rate. The free-surfaces in
354 Figure 7b at the maximum radius are not smooth due to the visualization package used to
355 visualize the model results, because the height of the lava flow is becoming close to the element
356 spacing, 1 meter for this model. Our results appear to behave in a similar fashion to experimental
357 models analyzed by *Buisson and Merle* [2002], that is once the lateral gravity-driven zone
358 develops, the shape of the central zone (dominated by the injection force) does not evolve further.
359 *Buisson and Merle* [2002] distinguish a juvenile and a mature dome growth stage with the dome
360 becoming mature once this central region is surrounded by a growing gravity-dominated region.
361 Unfortunately they do not include an image of their experimental model at different points in
362 time for us to compare our computational model against.
363
364 **3.2.2 Analysis of Dome Height Evolution**
365 To analyze our results for the maximum height of a Newtonian lava dome, considering an
366 injection dominated central region, we consider the dome height calculated by *Buisson and Merle*
367 [2002] in one of their experimental models as well as *Huppert et al.'s* [1982] analytical model.
368 Figure 8 shows a typical maximum height and radius evolution for one of our model runs in time
369 (Run 4, Table 1). This result shows that the final height of the lava dome is rapidly achieved. The
370 initial height level of the lava in the conduit was modeled to be 5 meters below the conduit exit
371 (see Figure 1). Therefore, there is a short period of time for the lava to reach the conduit exit at
372 h=0. While the lava dome height is increasing rapidly beyond h=0, the change in lava dome
373 radius is approximately linear with time due to the dome being in it juvenile stage [*Buisson and*
374 *Merle* 2002]. Once the increasing height of the lava dome slows and tends towards its asymptotic

limit the lava dome begins to spread predominantly laterally and the flow is then described by *Huppert et al.'s* [1982] theoretical model (Eqn. 8). The results are digitized in Figure 8 because the free-surface value is only being recorded at nodes in our model domain. However as the level-set function is a smooth and continuous function the free-surface of the lava dome also evolves smoothly.

Manipulating equations offered in *Huppert et al.* [1982] shows that the height of the extrusion has time-dependence as given by equation 9,

$$h = \alpha h^* t^{1/3}, \tag{9}$$

where α is a coefficient and h^* is a function of the extrusion rate and kinematic viscosity. This treatment suggests that the height should increase continuously with time, but our model runs show that the height asymptotically reaches its maximum value (Figure 8). That is, following the initially rapid growth in dome height the evolution of the dome is then predominantly laterally with height increasing only slightly. This is in agreement to experimental models considered by *Buisson and Merle* [2002, 2004] which show that in height against time experiments, for two-dimensional slot experiments with lubricated walls, after a time the maximum height tends to an equilibrium position.

The height of three of our model runs normalized by $h^* = \left(3\nu Q / g\right)^{1/4}$, as per *Huppert et al.'s* [1982] theoretical analysis, against time is shown in Figure 9 along with the theoretically

predicted result offered by *Huppert et al.* [1982] with $\alpha h^* = 0.02$. Figure 9 also shows the maximum dome height results from one of *Buisson and Merle's* [2002] experiments normalized by $h^* = \left(3\nu Q / g\right)^{1/4}$, against time. *Buisson and Merle's* [2002] model results show that the height of the dome does not evolve according to *Huppert et al.'s* [1982] relationship, instead they describe the maximum height evolution of the dome as asymptotic to an upper value. As for our model, the height of the dome only follows the relationship given by equation 9 for a small part of the evolution of the dome. Since *Buisson and Merle's* [2002] model run, shown in Figure 9, lasted only 80 hours it is difficult to fully ascertain if their dome had almost reached an equilibrium height, but the available results (more clearly presented in their 2002 paper) suggest this is most likely the case. The discrepancy between our model results and *Huppert et al.'s* [1982] theoretical analysis for the height of an evolving lava dome is probably because they do not consider a central uplift region due to injection. *Huppert et al.'s* [1982] analytical treatment over-simplifies dome growth and potentially neglects some significant physics.

Our results for the height evolution, Figures 8 and 9, can explain another cause for the departure from the theoretical predicted radius values offered by *Huppert et al.* [1982] analytical model in Figures 4 and 5 in the early stages of dome growth. For our lowest viscosity model (Run 5, $\eta=5\text{x}10^9$) in Figure 5 the modeled radius tends towards the theoretical trend given by *Huppert et al.* [1982] the most rapidly. This is because the model will begin to spread laterally the most rapidly due to a lower internal friction (viscosity) resulting in a smaller injection and gravity dominated central region. In contrast, in our highest viscosity model (Run6, $\eta=5\text{x}10^{10}$, Figure 5) the radius tends towards *Huppert et al.'s* [1982] theoretical trend the most slowly. This is due to a larger internal friction meaning the initial growth of the lava dome is governed predominantly by

the injection force and therefore this model has a large central region with lateral spreading occurring more slowly. After a time it is observed that all our results in Figures 4 and 5 follow *Huppert et al.'s* [1982] theoretically predicted trend, but only when the dome has a radius outside the influence of the central injection dominated region.

3.2.3 Ellipticity

Buisson and Merle [2002, 2004] use Lagrangian strain ellipses to describe the character of the flow observed in their experiments. The overall geometry of a mature lava dome is found to be a balance between injection from the conduit (upward movement) and gravity. *Buisson and Merle* [2002] locate a central area with inward shear sandwiched by a region of outward shear due to a change in sign in the velocity gradient as a result of the competition between injection and gravity forces. They also observe that once a lateral (gravity-dominated) zone develops the shape of the central zone does not change further with time. Observing the stretching trajectories in their model thus reveals a triple junction which defines an isotropic point in the strain field. To deduce if our strain pattern matches that observed by *Buisson and Merle's* [2002] we consider the axial ratio or measure of ellipticity, R, as given by equation 10.

$$R = \frac{1+\varepsilon_1}{1+\varepsilon_2} \tag{10}$$

The principal strains $\varepsilon_{1,2}$ are given by equation 11 where $\varepsilon_1 > \varepsilon_2$ and corresponds to the attitude of flattening planes.

$$\varepsilon_{1,2} = \frac{1}{2}\left(\varepsilon_{rr} + \varepsilon_{zz}\right) \pm \left[\varepsilon_{rz}^2 + \left(\frac{\varepsilon_{rr} - \varepsilon_{zz}}{2}\right)^2\right]^{1/2}, \quad (11)$$

and the angle φ which is obtained from the well known formula $\tan 2\varphi = \frac{2\varepsilon_{rz}}{\varepsilon_{rr} - \varepsilon_{zz}}$ represents the angle between the r-axis and the larger (less compressive) principal strains. We use an Eulerian or spatial definition for our strain measure ε_{ij}; the so called Almansi strain tensor [*Prager,* 1961] representing the strain at a fixed spatial position rather that the strain at a material point. The calculation of the Almansi strain is described in the appendix.

Because we are dealing with a highly deformable object in transit we consider the change in displacement over a fixed period of time. Figure 10 shows our computational model results for the calculated ellipticity at four points in the evolution of a lava dome with a viscosity of 2×10^9Pa s and an extrusion rate of $1.75 m^3 s^{-1}$. In Figure 10 the ellipticity for each image is calculated from the cumulative displacement over a time interval of 30 minutes. Ellipticity is shown in the figures as varying from 1.0 where the image is white to 1.2 where the image is black. The lava dome free-surface is represented as a smooth black line and the height of the volcano free-surface is at 20 meters (Figure 1). Outside of the lava dome the background is shaded to allow a better visual representation of the ellipticity within the dome. An ellipticity of 1 indicates no stretching and the principal axes are equal, whilst values of R increasing past 1.0 represent increasing levels of ellipticity. The maximum levels of ellipticity are much higher than 1.2 in Figure 10, principally in the region directly above the conduit exit, but a cut-off value was used to better show the ellipticity away from the region near the conduit exit. In agreement to *Buisson and Merle* [2002]

463 we observe an isotropic point in the strain field which shows no movement during dome growth.
464 Figure 10 shows the region where ellipticity remains equal to 1, to the right of the conduit and in
465 between the lava dome free-surface and base, which is also observed to remain stationary with
466 time once the central region has formed. Away from the central region shearing is predominantly
467 at the base of the dome due to the boundary condition of no slip at the volcano surface. In reality
468 the strain pattern will depend upon the rheology but we can consider this treatment as giving a
469 first-order approximation to what would be observed in nature.
470

471 **3.3 1979 Lava Dome on St. Vincent Soufrière, W.I.**

472 The 1971 and 1979 eruptions of Soufrière St. Vincent (W.I.) resulted in lava domes forming in
473 the volcano crater. During the 1979 eruption the crater floor was relatively dry and flat and the
474 eruption was documented extensively during the extrusion process. This eruption provides an
475 excellent opportunity to test our model against because the dome was extruded approximately
476 axisymmetrically suggesting endogenous growth. Table 2 provides the available data on the
477 radius, height and an estimate of the volume of the lava dome over time. The initial values for the
478 lava dome height and radius were based upon visual observations and therefore are likely to be
479 subject to large errors. Later measurements (from May 17th onwards) measurements were made
480 from the crater rim and are likely to be more accurate. Due to the method used to estimate the
481 volume, such that the upper surface is assumed to be flat and the margins slope at 35°, the
482 volume has an error associated with it of approximately 10%.
483

484 Figure 11 plots the available data for the height and radius of the dome as a function of time.
485 These data show that the extrusion rate appears to be relatively smooth, however in reality the

spreading was likely to be discontinuous. After May 12 1979 the maximum radius is an average of 7 values obtained from survey lines around the dome. The outer margins of the lava dome are also likely to be comprised of loose blocks, a talus, that have detached from the growing lava dome. We consider two techniques to model the growth of this lava dome, an increasing extrusion rate as described in *Huppert et al.* [1982] and a constant pressure-head model.

3.3.1 Increasing Extrusion Rate

The growth of the 1979 Soufrière St. Vincent lava dome is considered in a theoretical model developed by *Huppert et al.* [1982]. Following the same assumptions made in their analysis the beginning of the extrusion, when the lava was thought to behave as a freely flowing viscous fluid, is set to be 6th May 1979. They also propose that the volume data set is best represented by the relationship for the first 90 days of growth:

$$V = 0.0248t^{1.36} \tag{12}$$

Huppert et al. [1982] develop an analytical solution for a lava dome growing due to a variable extrusion rate and show that the radial extent of the flow is given by equation 13,

$$r_N = c(\alpha)\left(gS^3/3\nu\right)^{1/8} t^{(\alpha+1)/8}, \tag{13}$$

where $t^{\alpha}S$ is the volume of newly introduced fluid, $c(\alpha)$ is a constant given in the paper by *Huppert et al.* [1982] and S and α are prescribed constants. We consider the growth of the lava

dome using the parameters given by *Huppert et al*. [1982] and use a density of 2400kgm^{-3} for the lava. For the conduit we assume a radius of 50 meters and the time in the model equals zero when lava is extruded above the conduit exit. Figure 12 shows our model results for the height and radius obtained for differing viscosities against the observational data set as well as *Huppert et al.'s* [1982] best fit to the data for the radius, $r_H = 0.051t^{0.58}$

Huppert et al's [1982] analytical model result suggests that the viscosity of the lava dome was 2x10^{11}Pa s. Our model results do not fit well to the observational data set or to the best fit relationship given for the lava dome radius as derived by *Huppert et al.* [1982]. Generally our model results produce a dome whose central height is too great and none of the radius results fit particularly well to the observational data set. Also, in reality the surface of the lava dome will cool and crystallize resulting in blocks of lava falling from the dome surface creating a talus of loose blocky material ringing the dome. This effect may result in a larger radius than theoretically modeled.

Because *Huppert et al.'s* [1982] analytical model doesn't consider uplift in the centre of the dome, due to the influx of lava, or an additional resisting force due to the talus it is likely that the effective viscosity for the lava dome has been over-estimated. The viscosity for the lava extruded during this eruption period from petrological estimates in *Huppert et al.'s* [1982] paper suggests a viscosity varying from approx 2.1x10^7 to 8.1x10^{10} Pa s for temperatures between 1000 and 700°C. The lava from the Soufrière St. Vincent volcano was thought to have been erupted with a temperature of approximately 1000°C (±100°C). Naturally there will be some cooling at the

surface of the dome, but due to the low thermal conductivity of the lava this cooled layer will not penetrate far into the dome and will be on the order of meters [*Huppert et al.* 1982].

Our modeled lava dome radius, using the approximation to the volume data set for the first 90 days of growth given by *Huppert et al.* [1982], appears to progressively depart from the observational data set. This model would predict that dome growth should continue indefinitely. A more appropriate model may be to consider dome growth using a fixed pressure head from the conduit inlet and we consider this model next.

3.3.2 Constant Pressure-Head Model

During and after June 1979 the volume discharge rate for the lava dome was observed to decrease almost linearly with the height of the flow, consistent with the hypothesis of a pressure head driving the extrusion. As the pressure from below was increasingly balanced by the hydrostatic pressure of the lava itself, the lava would stop flowing from the conduit exit when the lava column reached hydrostatic pressure equilibrium. A decrease in driving pressure in the magma chamber could also result in a decrease in extrusion rate, although this is likely to occur over much longer time scales due to the size of the magma chamber with respect to the volume of extruded lava. *Huppert et al.* [1982] discuss that such a pressure-head could be responsible for the decreasing extrusion rate at later times in the evolution of the dome. Figure 13 shows the observed extrusion rate with height for the lava dome. The extrusion rate and day in the eruption are calculated considering adjacent values in Table 2. Following a height of 75.5 meters there is an approximately linear decrease in extrusion rate, shown in Figure 13 as a dashed linear line. The linear fit in Figure 13 ignores the initial data point at a height of approximately 50 meters.

553 This is because at the beginning of the eruption the lava would have had to force its way through
554 a conduit blocked by ejecta, debris and cooled lava and this would explain the initially lower
555 extrusion rate. Following this initial period the lava could be considered as flowing freely.
556
557 Considering the extrusion rate as a function of time in Figure 14 we can extrapolate an initial
558 extrusion rate when the lava was approximately behaving as a freely flowing fluid. Using the
559 approximated volume at the first reliable data point, day 13.5 (i.e. $7.1 \times 10^6 m^3$), and the gradient of
560 the extrusion rate we calculate that the initial extrusion rate was approximately $10.5 m^3 s^{-1}$ and
561 began on day 5 (12^{th} May 1979). Using similar assumptions *Huppert et al.* [1982] reached the
562 conclusion that the extrusion began to flow freely on 14^{th} May 1979, day 7. Figure 14 also
563 suggests that the pressure-head model is only appropriate for the first 90 days of lava dome
564 growth because after this time the extrusion rate would fall to zero.
565
566 Our computational model applies a constant stress (pressure) boundary condition at the conduit
567 inlet such that the initial extrusion rate is approximately $10.5 m^3 s^{-1}$ at the height of the conduit
568 exit. The conduit radius is 50 meters, the length of the conduit in the model is modeled to be 50
569 meters and the modeled lava has a density of $2400 kgm^{-3}$. Table 3 shows the values used for the
570 different model runs and Figure 15 shows our results for the height above the conduit exit and
571 radius against time along with the observational data set and Huppert et al.'s best fit relationship
572 for the radius. Our model results for the height and radius of the lava dome extruded on Soufrière
573 St. Vincent in 1979 show a closer agreement to the observational data points in the constant
574 applied pressure head model (Figure 15) than for the fixed extrusion rate model considered by
575 *Huppert et al.* [1982] (Figure 12). For example, the model radius results for a constant pressure

fit more closely to Huppert et al.'s best fit relationship than for the fixed extrusion rate model. Also the height of the dome reaches an asymptotic limit as suggested by the observational data set, which is achieved in the constant pressure model but not in the fixed extrusion rate model in which the height continues to increase.

It is interesting to observe how the maximum radius evolves with time for the different viscosities used for the lava. The model run with the lowest viscosity, 10^{10} Pa s (Run1, Table 3), shows that for an applied pressure which produces an extrusion rate initially equal to $10.5 m^3 s^{-1}$ at the conduit exit, the radius fits reasonably well to the observational data set. Considering the same viscosity, Run 1, in Figure 12 it is observed that the radius rapidly departs from the data set. The difference in the model results is due to the change in extrusion rate over time and Figure 16 shows this change in extrusion rate against the available observational data.. Despite the radius in Run1 (Table 3, Figure 15) being a reasonably good fit to the observational data the modeled lava dome height does not fit at all to the observational data set and is too low.

For the highest viscosity model run, $2x10^{11}$ Pa s (Run4, Table 3), which produces an extrusion rate initially equal to $10.5 m^3 s^{-1}$ at the conduit exit, the modeled radius also fits well to the observational data set. In fact this model run result lies almost exactly on the best fit relationship for the lava radius derived by *Huppert et al.* [1982]. However the modeled height of the lava dome is observed to be too large when compared to the observational data set at later times in the history of the dome. The model runs with viscosities in between these values produce radii and height values between the values given by Run1 and Run4.

599 Our simple lava dome model does not capture the observational height or dome radius well and
600 this is partly because there are other processes at work. As the lava dome on Soufrière St. Vincent
601 grows we need to consider that the free-surface will cool, resulting in the detachment of blocks
602 that will accumulate on the dome surface and flow margins creating a talus. As a consequence it
603 is likely that in the initial stages of lava dome growth the height is lower than theoretically
604 expected due to detachment of these loose rocks from the free surface. This same process may act
605 to increase the observed radius due to the accretion of these loose blocks which have tumbled
606 down the flanks towards the front of the flow. This means that initially the lateral extent of the
607 lava dome will be larger than the massive continuous lava complex at the centre of the dome
608 which is what we model here.
609
610 At later times in the evolutionary history of the lava dome the radius may be less than
611 theoretically predicted due to the resistance created by the loose avalanching rocks blocking the
612 lateral flow of the dome. Such a talus could cause a substantial radial resistance which is not
613 considered in our models but may act to slow the spreading rate. In addition to this the lateral
614 spreading may also slow due to the crater floor not being smooth. The maximum height at the
615 centre of the dome may become supported by the surrounding lava and therefore may be slightly
616 higher than theoretically predicted due to spines and individual lava lobes thrust out at the top of
617 the dome.
618
619 With these processes in mind, our model result that best fits the observational data set is Run2
620 with an effective viscosity of 5×10^{10} Pa s. This viscosity value is within the range suggested by
621 *Huppert et al.* [1982] from petrological studies and suggests an effective temperature of

622 approximately 715°C. Since the lava was thought to be erupted with a temperature of
623 approximately 1000°C (±100°C) this result suggests that cooling at the free-surface,
624 crystallization and viscosity gradients within the dome are very important to the evolution of the
625 dome.
626
627 None of the model runs for the extrusion rate against time (Figure 16) fit the observational data
628 set very well. It is uncertain whether this is due to inaccuracy with the data set or with the
629 simplicity of our model. Observational extrusion rates are hard to achieve, as shown by the
630 scatter in the observational data set, due to the difficulty associated with obtaining accurate
631 volumetric values [*Wadge et al.,* 2005]. There is some discrepancy between Figures 13 and 14,
632 such that extrapolating the linear fit for the height against extrusion rate of the Soufrière St.
633 Vincent 1979 lava dome back to the beginning of the eruption, when the height is zero, would
634 give a very large extrusion rate. Without a better data set it is difficult to extract the actual
635 extrusion rates with time. Therefore it is difficult to relate the observational data for the extrusion
636 rate to our modeled extrusion rate.
637
638 **3.4 October 1980 Lava Dome Growth on Mount St. Helens, USA**
639 The lava dome that grew during 18th and 19th October 1980 on Mount St. Helens, USA, is
640 another suitable test case because it grew as a simple, near axisymmetric dome on a relatively
641 unconstrained surface and its growth was measured albeit sparsely [*Moore et al.,* 1981]. The lava
642 dome was emplaced immediately following the blasting away of a pre-existing dome, excavating
643 a shallow depression approximately 250 m in diameter and providing a near-horizontal plane for
644 the dome to grow upon. Its initial stages of growth were observed three times and again after

about 19 hours when the lava supply had stopped when it was approximately 50 m in maximum height and 185 m in diameter [*Moore et al.,* 1981]. Over the following week the dome spread and sagged considerably. Here we assume that lava supply stopped at 19 hours into the eruption when the fourth observation was made.

As for the Soufrière St. Vincent lava dome model we assume an effective viscosity for the lava. According to *Murase et al.* [1984] the temperature of the extruded lava was probably somewhere between 900 and 1000°C giving a viscosity of between 10^8Pa s and 10^{14}Pa s for the minimum and maximum crystal volume fractions permissible respectively [*Cashman,* 1992; *Murase et al*. 1984]. However, estimates of the viscosity of the dome from the observed flow of lobes by the U. S. Geological Survey suggest viscosities in the range of 10^9 to 10^{10}Pa s [*Murase et al.,* 1981]. The total volume erupted in this dome building event was approximately 1.2 million cubic meters from estimates of the final dome shape. This gives a constant extrusion rate approximately equal to 17.5 m^3s^{-1} over the 19 hour extrusion period, although it is not likely to have been constant during this time. The density of the dome is assumed to be 2400 kgm^{-3} [*Murase et al.* 1984] and the conduit radius is modeled to be 15 meters [*Moore et al.,* 1981]. Table 4 lists the parameters used in our model runs. For this analysis we consider lava dome growth due to a constant extrusion rate as well as a pressure driven flow using appropriate boundary conditions at the conduit inlet. Figure 17 shows the results from our model runs along with the available observational data.

Results for the model runs using a constant extrusion rate as the conduit inlet boundary condition show a large over-shoot in the initial height of the lava dome (Figure 17). This is due to the lava

668 being extruded relatively rapidly and the height increasing much more rapidly than the dome can
669 spread laterally. Once lateral spreading has exceeded a certain radius (observed to be greater than
670 twice the conduit radius) the maximum height of the lava dome begins to stabilize to a constant
671 value. The radius and height are both observed to be too large for the constant extrusion rate
672 models. This may be due to the free-surface not fitting the actual lava dome shape or the final
673 volume being a poor estimate and thus the extrusion rate also being over-estimated.
674
675 Results for the model runs using a constant applied pressure produce results closer to the
676 observational data set. Run 4, having a viscosity of $2x10^9$ Pa s produces the best fit to the data set.
677 The final maximum radius is slightly smaller than that observed at 19 hours after the eruption
678 began, but this is to be expected if we consider that a talus was surrounding the dome. Our model
679 results using a constant driving pressure as the inlet boundary condition show very little over-
680 shoot in the initial height of the lava dome. Only Run 6 shows a slight decrease from its initial
681 height and this is due to the relatively large pressure and hence a maintained extrusion rate with
682 time (Figure 18). The modeled maximum radius, in the constant driving pressure runs, departs
683 from the constant applied extrusion rate model runs at later times. However a couple of the
684 constant driving pressure and constant extrusion rate models show very similar radius values
685 initially which only depart at later times due to the large difference in height of the dome in the
686 central region.
687
688 *Murase et al.* [1984] apply *Huppert et al.'s* [1982] analytical model for the height and radius of
689 the lava dome extruded on Mount St. Helens in late 1981 to calculate an effective viscosity.
690 Although we have considered the 1980 lava dome growth, the rheology of the lava was relatively

691 consistent during the dome building phase and would not have changed substantially. *Huppert et*
692 *al.'s* [1982] analytical model suggests that the viscosity of the lava was 5.1×10^{15} Pa s, while
693 *Murase et al.'s* [1984] petrological analysis of dome rock suggest a viscosity of between 10^8 Pa s
694 and 10^{14} Pa and observations of dome lobes by the U. S. Geological Survey suggest viscosities in
695 the range of 10^9 to 10^{10}Pa s [*Murase et al.,* 1981]. These values are closer to our computational
696 model result which suggests an effective viscosity for the entire lava dome of 2×10^9 Pa s.
697

698 **4. Conclusions**

699 The evolution of a lava dome is governed predominantly by its effusion rate and rheology. There
700 are a large number of parameters that influence the rheology of the lava with the most influential
701 parameters being: temperature, melt composition, pressure, applied stress, volatile content and
702 composition, bubble fraction and size as well as crystal content. It is unrealistic to model the
703 growth of a lava dome using a constant effective viscosity but our treatment of lava dome growth
704 has been deliberately simplified to show the capability of the level-set method. The level-set
705 method has been shown to be a technique robust enough to model the free-surface of a growing
706 lava dome. This technique is not only computationally light but does not require an initial above-
707 ground free-surface from which the dome can be grown. *Hale and Wadge* [2003] observed that
708 assuming an initial lava free-surface shape can influence the final shape and evolution of the
709 dome, whereas this technique avoids the complication of an initial condition. From this
710 simplified treatment of endogenous lava dome growth it will be possible to include empirical
711 rheological models which can advance the model and include history-dependent effects and latent
712 heat release. This will be achieved by introducing an elastic membrane to capture the solid

carapace on a lava flow. The level-set method can also consider multiple surfaces and discontinuities which can be used to consider exogenous lava dome growth.

Our models have shown that the computation of a lava dome free-surface and internal flow properties requires consideration of lava injection forces as well as the influence of gravity. Therefore an analytical study is not adequate to capture the physics. In addition to this, models that consider a constant pressure head show that the extrusion rate automatically decreases as per the observational data. However additional processes such as a resisting force due to talus and yield strength in the upper surface of the dome need to be considered to capture the evolution of the dome more accurately.

Appendix:

Governing Equations

The constitutive equation for a Newtonian, viscous material reads:

$$\sigma'_{ij} = 2\eta D'_{ij} \qquad \text{(A1)}$$

where

734
$$\begin{aligned} \sigma'_{ij} &= \sigma_{ij} - P\delta_{ij} \quad and \quad P = -\frac{1}{3}\sigma_{kk} \\ D'_{ij} &= D_{ij} - d\delta_{ij} \quad and \quad d = -\frac{1}{3}D_{kk} \end{aligned} \tag{A2}$$

735

736 where σ_{ij} is the stress, η the viscosity, D_{ij} the stretching, δ_{ij} is the Kronecker delta and P the
737 pressure. We assume $P_{,t} = -KD_{kk}$; K is the bulk modulus of the lava or air respectively and $(\cdot)_{,t}$
738 means partial differentiation with respect to time. The stress-equilibrium equations in axi-
739 symmetrical coordinates reads

740

741
$$\begin{aligned} \widetilde{\sigma_{rr}}_{,r} + r\sigma_{rz,z} - \sigma_{\theta\theta} + rf_r &= 0 \\ r\sigma_{zz,z} + \widetilde{\sigma_{rz}}_{,r} + rf_z &= 0 \end{aligned} \tag{A3}$$

742

743 Insertion of A1, A2 yields:

744

745
$$\begin{aligned} &\left(r\left(2\eta_\alpha v_{r,r} - P^t + (\Delta t K_\alpha - \frac{2}{3}\eta_\alpha)(v_{r,r} + v_{z,z} + \frac{v_r}{r}) \right) \right)_{,r} + r\widetilde{\eta_\alpha (v_{r,z} + v_{z,r})}_{,z} - \\ &-2\eta_\alpha \frac{v_r}{r} + P^t - (\Delta t K_\alpha - \frac{2}{3}\eta_\alpha)(v_{r,r} + v_{z,z} + \frac{v_r}{r}) + rf_r^\alpha = 0 \\ &r\left(2\eta_\alpha v_{z,z} - P^t + (\Delta t K_\alpha - \frac{2}{3}\eta_\alpha)(v_{r,r} + v_{z,z} + \frac{v_r}{r}) \right)_{,z} + \widetilde{\eta_\alpha (v_{r,z} + v_{z,r})}_{,r} + rf_z^\alpha = 0 \end{aligned} \tag{A4}$$

746

747 Where $\alpha = 1$ corresponds to lava and $\alpha = 2$ to the embedding medium. In A4 the differential
748 constitutive relationship for the pressure has been replaced by

749

$$\tilde{v}_i = \frac{Q}{\pi a^2} v_i,\ \tilde{x}_i = \frac{1}{a} x_i,\ \tilde{P} = \frac{\pi a^3}{\eta_{lava} Q} P,\ \tilde{t} = \frac{\pi a^3}{Q} t, \tag{A5}$$

where Q is either given or, as in the case of the constant pressure head boundary condition, defined as : $Q = \pi a^3 P^0 / \eta_{lava}$. Insertion into A4 and dropping tildes and assuming $f_r^\alpha = 0$ and $f_z^\alpha = \rho_\alpha g$ gives, with respect to the dimensionless coordinates:

$$\begin{aligned}
&\left(r\left(2v_{r,r} - \frac{\eta_{lava}}{\eta_\alpha} P^t + (\frac{\pi a^3 K_\alpha / \eta_\alpha}{Q} \Delta t - \frac{2}{3})(v_{r,r} + v_{z,z} + \frac{v_r}{r}) \right) \right)_{,r} + r\left(v_{r,z} + v_{z,r} \right)_{,z} \\
&- 2\frac{v_r}{r} + \frac{\eta_{lava}}{\eta_\alpha} P^t - (\frac{\pi a^3 K_\alpha / \eta_\alpha}{Q} \Delta t - \frac{2}{3})(v_{r,r} + v_{z,z} + \frac{v_r}{r}) = 0 \\
&r\left(2v_{z,z} - \frac{\eta_{lava}}{\eta_\alpha} P^t + (\frac{\pi a^3 K_\alpha / \eta_\alpha}{Q} \Delta t - \frac{2}{3})(v_{r,r} + v_{z,z} + \frac{v_r}{r}) \right)_{,z} + \\
&+ r\left(v_{r,z} + v_{z,r} \right)_{,r} + \frac{\pi a^4 \rho_\alpha g r}{\eta_\alpha Q} = 0
\end{aligned} \tag{A6}$$

Escript Formulation

The modeling library *escript* has been developed as a module extension of the scripting language Python to facilitate the rapid development of 3-D parallel simulations on the Altix 3700 [*Davies et al*, 2004]. The finite element kernel library, *Finley*, has been specifically designed for solving large-scale problems on ccNUMA architectures and has been incorporated as a differential equation solver into *escript*. In *escript* Python scripts orchestrate numerical algorithms which are implicitly parallelised in *escript* module calls, without low-level explicit threading implementation by the *escript* user.

The *escript* Python module provides an environment to solve initial boundary value problems (BVPs) problems through its core finite element library *Finley*. A steady, linear second order BVP for an unknown function u is processed by *Finley* in the following templated system of PDEs (expressed in tensorial notation):

$$-(A_{ijkl}v_{k,l})_{,j} - (B_{ijk}v_k)_{,j} + C_{ikl}v_{k,l} + D_{ik}v_k = -X_{ij,j} + Y_i . \quad \text{(A7)}$$

where the Einstein summation convention is used. *Finley* accepts a system of natural boundary conditions given by:

$$n_j(A_{ijkl}v_{k,l} + B_{ijk}v_k) + d_{ik}v_k = n_j X_{ij} + y_i \text{ on } \Gamma_i^N \quad \text{(A8)}$$

where n denotes the outer normal field of the domain and A, B and X are as for (1). d and y are coefficients defined on the boundary. The Dirichlet boundary condition is also accepted:

$$u_i = r_i \text{ on } \Gamma_i^D \quad \text{(A9)}$$

where r_i is a function defined on the boundary. *Finley* computes a discretisation of (1) from the variational formulation. The variational problem is discretised using isoparametric finite elements on unstructured meshes. Available elements shapes are line, triangle, quadrilateral, tetrahedron and hexahedron of orders one and two.

With both the *escript* and *Finley* technologies, complex models and very large simulations can be rapidly scripted and run easily. The code is fully portable, but optimized at this stage for the local SGI ALTIX super cluster.

Putting A6 in the shape of the PDE 1 yields:

$$A_{ijkl} = r((\frac{\pi a^3 K_\alpha / \eta_\alpha}{Q}\Delta t - \frac{2}{3})\delta_{ij}\delta_{kl} + (\delta_{ik}\delta_{jl} + \delta_{il}\delta_{jk})) \quad \text{(A10)}$$

$$B_{ijk} = (\frac{\pi a^3 K_\alpha / \eta_\alpha}{Q}\Delta t - \frac{2}{3})\delta_{ij}\delta_{k0}$$

$$C_{ikl} = (\frac{\pi a^3 K_\alpha / \eta_\alpha}{Q}\Delta t - \frac{2}{3})\delta_{kl}\delta_{i0}$$

$$D_{ik} = \frac{1}{r}(\frac{\pi a^3 K_\alpha / \eta_\alpha}{Q}\Delta t - \frac{4}{3})\delta_{i0}\delta_{k0}$$

$$X_{ij} = r\frac{\eta_{lava}}{\eta_\alpha}P^t\delta_{ij}$$

$$Y_i = \frac{\eta_{lava}}{\eta_\alpha}P^t\delta_{i0} + \frac{\pi a^4 \rho_\alpha g r}{\eta_\alpha Q}\delta_{i1}$$

Where the indexes are 0 for the r coordinates and 1 for the z coordinates.

Almansi Strain Tensor

The cartesian components of the Almansi strain tensor [*Prager,* 1961] are defined as:

808 $$\varepsilon_{ij} = \frac{1}{2}(u_{i,j} + u_{j,i} - u_{k,i}u_{k,j})$$

809 We write out the rr, zz and rz components for easy reference:

810

811 $$\varepsilon_{rr} = u_{r,r} - \frac{1}{2}(u_{r,r}^2 + u_{z,r}^2),\ \varepsilon_{zz} = u_{z,z} - \frac{1}{2}(u_{z,z}^2 + u_{r,z}^2),\ \varepsilon_{rr} = \frac{1}{2}(u_{r,z} + u_{z,r} - (u_{r,r}u_{r,z} + u_{z,z}u_{z,r}))$$

812

813 The displacements $u_i(\mathbf{x},t)$ are obtained as follows:

814

815 $u_i^{t+\Delta t} = u_i^t - v_k^{t+\Delta t}u_{i,k}^t\Delta t + v_k^{t+\Delta t}\Delta t$ +upwind terms [*Zienkiewicz and Taylor,* 2000].

816

Acknowledgments

Support is gratefully acknowledged by the Australian Computational Earth Systems Simulator Major National Research Facility (ACcESS MNRF), the Queensland State Government, The University of Queensland, and SGI. The Australian Commonwealth Government, participating institutions, and the Victorian State Government fund the ACcESS MNRF. Hans Mühlhaus and Laurent Bourgouin would also like to acknowledge the partial support from the ARC discovery grant DP0346039 "Computer simulation to study emergence of material texture in the Earth and Plate Tectonics". We also thank the two reviewers, Boris Behncke and Julien Vaucher, for suggesting improvements to the original paper.

827 **References**

828 Balmforth, N. J., A. S. Burbridge and R. V. Craster, (2001), Shallow lava theory, in
829 *Geomorphological Fluid Mechanics* edited by N. J. Balmforth and A. Provenzale, pp. 164-187,
830 Springer-Verlag, New York.
831 Buisson C. and O. Merle (2002), Experiments on internal strain in lava dome cross sections. *Bull.*
832 *Volcanol., 64* (6), 363-371.
833 Buisson C. and O. Merle (2004), Numerical simulation of strain within lava domes. *J. Struct.*
834 *Geol., 26* (5): 847-853.
835 Cashman, K. V. (1992), Groundmass crystallization of Mount St. Helens dacite, 1980-1986: A
836 tool for interpreting shallow magmatic processes, *Contrib. Mineral. Petrol., 109* (4): 431-449.
837 Davies, M., L. Gross and H.-B. Mühlhaus (2004), Scripting High Performance Earth Systems
838 Simulations on the SGI Altix 3700, *7th Intl Conf. on High Performance Computing and Grid in*
839 *Asia Pacific Region, Tokyo,* August 2004, 244-251.
840 Griffiths, R. W. (2000), The dynamics of lava flows, *Annu. Rev. Fluid Mech.,* 31, 477 – 518.
841 Griffiths, R. W. and J. H. Fink (1993), Solidifying Bingham extrusions: a model for the growth of
842 silicic lava domes. *J. Fluid Mech., 347,* 13-36.
843 Hale A. J. and G. Wadge (2003), Numerical modeling of the growth dynamics of a simple silicic
844 lava dome *Geophys. Res. Letts., 30* (19): Art. No. 2003 OCT 10.
845 Huppert, H. E., J. B. Shepherd, H. Sigurdsson, et al. (1982), On lava dome growth with
846 application to the 1979 lava extrusion of the Soufriere St. Vincent. *J. Volcanol. Geotherm. Res.,*
847 *14* (3-4): 199-222.
848 Iverson, R. M., (1990), Lava domes modeled as brittle shells that enclose pressurized magma,
849 with application to Mount St. Helens, in *Lava flows and domes; emplacement mechanisms and*
850 *hazard implications* edited by J. H. Fink, pp. 47-69, Springer-Verlag, New York.
851 Melnik, O. E. and R. S. J. Sparks, (1999), Non-linear dynamics of lava dome extrusion. *Nature*
852 *402*, 37-41.
853 Melnik, O. E. and R. S. J. Sparks, (2005), Controls on conduit magma flow dynamics during lava
854 dome building eruptions. *J. Geophys. Res. 110(B02209)*: doi:10.1029/2004JB003183.
855 Moore, J. G., P. W. Lipman, D. A. Swanson and T. R. Alpha (1981), Growth of the lava domes
856 in the crater, June 1980 – January 1981. The 1980 Eruptions of Mount St. Helens, Washington,
857 *U.S. Geol. Surv. Prof. Pap.*, 1250, edited by Lipman, P. W. and D. R. Mullineaux, 541-547.
858 Murase, T., A. R. McBirney and W. G. Melson (1984), Viscosity of the lava dome on Mount St.
859 Helens, *Bull. Volcanol., 24*, 193-204.
860 Osher S. and J. A. Sethian (1988), Fronts propagating with curvature-dependent speed –
861 Algorithms based on Hamilton-Jacobi formulations. *J. Comp. Phys., 79* (1): 12-49.
862 Prager, W. (1961), *Introduction to Mechanics of Continua*, Boston, MA: Ginn.
863 Sussman, M., P. Smereka and S. Osher (1994), A level set approach for computing solutions to
864 incompressible two-phase flow. *J. Comp. Phys., 114*, 146-159.
865 Voight, B. (2000), Structural stability of andesite volcanoes and lava domes, *Phil. Trans. Roy.*
866 *Soc. Lon. A, 358* (1770): 1663-1703.
867 Wadge, G. D. G. Macfarlane, D. A. Robertson, et al. (2005), AVTIS : A novel millimetre-wave
868 ground based instrument for volcano remote sensing. *J. Volcanol. Geotherm. Res., 146 (4)*: 307-
869 318
870 Zienkiewicz, O.C. and Taylor, R.L. (2000), *The Finite Element Method, Volume 3: Fluid*
871 *Mechanics*, 5th ed., Butterworth-Heinemann
872

873 **Figure captions**

874 Figure 1: The axisymmetric domain used in our computational model with the free-surface for
875 two time-steps t=0 and t=tn shown as a dashed line. The curved arrow at the top left of each
876 image represents the rotation axis about r=0. This domain set-up models the flow of lava in the
877 upper conduit and free-surface of the volcano. The shaded region at the bottom-right of the
878 domain corresponds to the surface of the volcano and has the boundary condition of zero velocity
879 and a height of h. The radius of the conduit is a, and the lava inlet boundary condition in the
880 model is applied at the conduit inlet.

881

882 Figure 2: Five isosurfaces of ϕ at distances of -2m, -1m, 0m, 1m and 2m around the zero level
883 set value after four hundreds time steps. The model domain contains 60 by 60 order two
884 elements, *i.e.* 11041 nodes, and the dimension of the domain is 60m x 60m.

885

886 Figure 3: Modeled volume (continuous line) against theoretical volume (dashed line) for one run
887 of lava dome growth. Due to the slight compressibility of the modeled lava there is a 3% volume
888 loss.

889

890 Figure 4: Normalised radius against time for our computational model, Runs 1 to 3 with varying
891 extrusion rate. The parameters used for the different runs are given in Table 1. The analytical
892 model result of *Huppert et al.* [1982] is shown as a dashed line.

893

Figure 5: Normalised radius against time for our computational model, Runs 4 to 6 with varying viscosity. The parameters used for the different runs are given in Table 1. The analytical model result of *Huppert et al.* [1982] is shown as a dashed line.

Figure 6: A cartoon of lava dome split into two flow domains; injection and gravity driven, and gravity-only driven flow.

Figure 7: Results from our computational model for the evolution of a lava dome free surface with a viscosity of $2x10^9$ Pa s. The base of the volcano is at 20 metres and the conduit radius is 15 metres. The horizontal line in both figures at z=15 metres is the initial height of the level-set. In figure a) the extrusion rate is $17.5m^3s^{-1}$, whilst in figure b) it is $0.175m^3s^{-1}$. The time-difference between each surface corresponds to approximately 100 minutes and 52 hours, for figures a and b respectively. The axis of rotation is at r=0.This figure shows how the two domains, injection plus gravity and gravity-only dominated, evolve.

Figure 8: Typical lava dome maximum radius and height against time obtained from one of our computational model runs (Run 4, Table 1). The maximum radius is given by the solid black line and the left axes, whilst the maximum height is given by the solid grey line and the right axes.

Figure 9: Normalised height against time for three model runs (Run 2, Run 4, Run6; Table 1) with the key for each run shown in the figure. The short-dashed line is the theoretically predicted height of the dome according to the *Huppert et al.* [1982] model. The open circles shows the

results from one of *Buisson and Merle's* [2002] experiments in which they describe the maximum height of the dome as asymptotic to an upper value.

Figure 10: Measure of ellipticity for a lava dome with a viscosity of $2x10^9$Pa s and an extrusion rate of $1.75m^3s^{-1}$. Figures a to d show a series of times shots during the growth of the lava dome with ellipticity calculated from the cumulative displacements over a time interval of 30 minutes in each figure. The value of ellipticity is shown from 1 (white) to 1.2 (black). The horizontal axis corresponds to r and the vertical axis to z with the black line showing the outline of the lava dome. The volcano surface is at a height of 20 meters and the conduit radius is 15 meters with the domain rotated about r=0

Figure 11: Height at the centre of the Soufrière St. Vincent 1979 lava dome above the crater floor and average maximum radius against time.

Figure 12: Our computational model results for the growth of the 1979 Soufrière St. Vincent lava dome using *Huppert et al's* [1982] extrusion rate function against time. Triangles and circles in the figure represent the observational data for the radius and height respectively. The continuous lines for our model results correspond to the maximum radius values, whilst the shaded lines are for the height. The dashed line shows the best-fit relationship derived by *Huppert et al.* [1982] for the radius of the lava dome in the first 90 days of growth.

Figure 13: Extrusion rate against height for the Soufrière St. Vincent 1979 lava dome extracted from the volume values given in Table 2. The dashed line shows the linear trend for the extrusion rate to decrease with increasing dome height.

Figure 14: Extrusion rate against day in the eruption of the Soufrière St. Vincent 1979 lava dome extracted from the volume values given in Table 2. The dashed line shows the linear trend for the extrusion rate to decrease with time.

Figure 15: Our computational model results for the growth of the 1979 Soufrière St. Vincent lava dome using a constant pressure-head (stress) applied at the inlet boundary against time. Triangles and circles in the figure represent the observational data for the radius and height respectively. The continuous lines for our model results correspond to the maximum radius values, whilst the shaded lines are for the height. The dashed line shows the best-fit relationship derived by *Huppert et al.* [1982] for the radius of the lava dome in the first 90 days of growth.

Figure 16: Modeled extrusion rate for the model runs shown in Figure 15, for the growth of the 1979 Soufrière St. Vincent lava dome using a constant pressure-head at the inlet boundary, against time. The extrusion rate against day in the eruption extracted from the volume values given in Table 2 along with a 10% uncertainly are shown as triangles.

Figure 17: Our computational model results (parameters as given in Table 4) for the growth of the October 1980 Mount St. Helens lava dome against time. These model runs consider either a constant pressure-head (stress) or a fixed extrusion rate applied at the inlet boundary. Squares and

960 circles in the figure represent the observational data for the radius and height respectively. The
961 continuous lines for our model results correspond to the maximum radius values, whilst the
962 shaded lines are for the height. The dashed line shows the best-fit relationship derived by
963 *Huppert et al.* [1982] for the radius of the lava dome in the first 90 days of growth.
964
965 Figure 18: Modeled extrusion rate for the model runs shown in Figure 17, for the growth of the
966 October 1980 Mount St. Helens lava dome (parameters as given in Table 4).
967

968 **Tables**

969 Table 1: List of parameters used in our model runs for the comparison against the analytical
970 model result of *Huppert et al.* [1982].

Model run	Extrusion rate (m^3s^{-1})	Lava viscosity (Pa s)
1	0.0625	10^{10}
2	0.125	10^{10}
3	0.25	10^{10}
4	0.125	$2x10^{10}$
5	0.125	$5x10^{9}$
6	0.125	$5x10^{10}$

971

972 Table 2: Observational data for the lava dome extruded on Soufrière St. Vincent 1979.

Date	Day	Radius (m)	Height (m)	Volume (m^3)
07.05.79	1	30	30	8.5×10^4
17.05.79	8	150	69	2.3×10^6
25.05.79	19	275	82	11.9×10^6
18.06.79	43	363	100	26.2×10^6
02.07.79	57	378	117	31.2×10^6
10.07.79	65	394	117	35.0×10^6
14.07.79	69	394	120	35.4×10^6
04.08.79	90	410	123	39.5×10^6
14.08.79	100	413	131	41.4×10^6
21.08.79	107	415	131	41.9×10^6
01.09.79	118	418	132	42.7×10^6
04.09.79	121	420	132	43.3×10^6
07.09.79	124	421	132	43.6×10^6
15.09.79	132	424	132	44.6×10^6
23.09.79	140	429	133	46.1×10^6
02.10.79	149	434	133	47.3×10^6

973

974 Table 3: Parameters used in our model runs for the growth of the lava dome extruded on St.
975 Vincent Soufrière 1979 with a constant pressure head.

Model run	Stress applied Pa (50 meters below conduit exit).	Lava viscosity (Pa s)
1	$2.61x10^6$	10^{10}
2	$9.10x10^6$	$5x10^{10}$
3	$17.00x10^6$	10^{11}
4	$33.0x10^6$	$2x10^{11}$

976

977 Table 4: List of parameters used in our model runs for the growth of the lava dome extruded on
978 Mount St. Helens, USA, October 1980.

Run	Inlet boundary condition	Lava viscosity (Pa s)
1	$Q = 17.5\ m^3s^{-1}$	$2x10^9$
2	$Q = 17.5\ m^3s^{-1}$	$4x10^9$

3	$\sigma_{zz} = 15.0 \times 10^6$	10^9
4	$\sigma_{zz} = 20.0 \times 10^6$	2×10^9
5	$\sigma_{zz} = 25.0 \times 10^6$	2×10^9
6	$\sigma_{zz} = 30.0 \times 10^6$	2×10^9

979
980

981 **Figures**
982 1

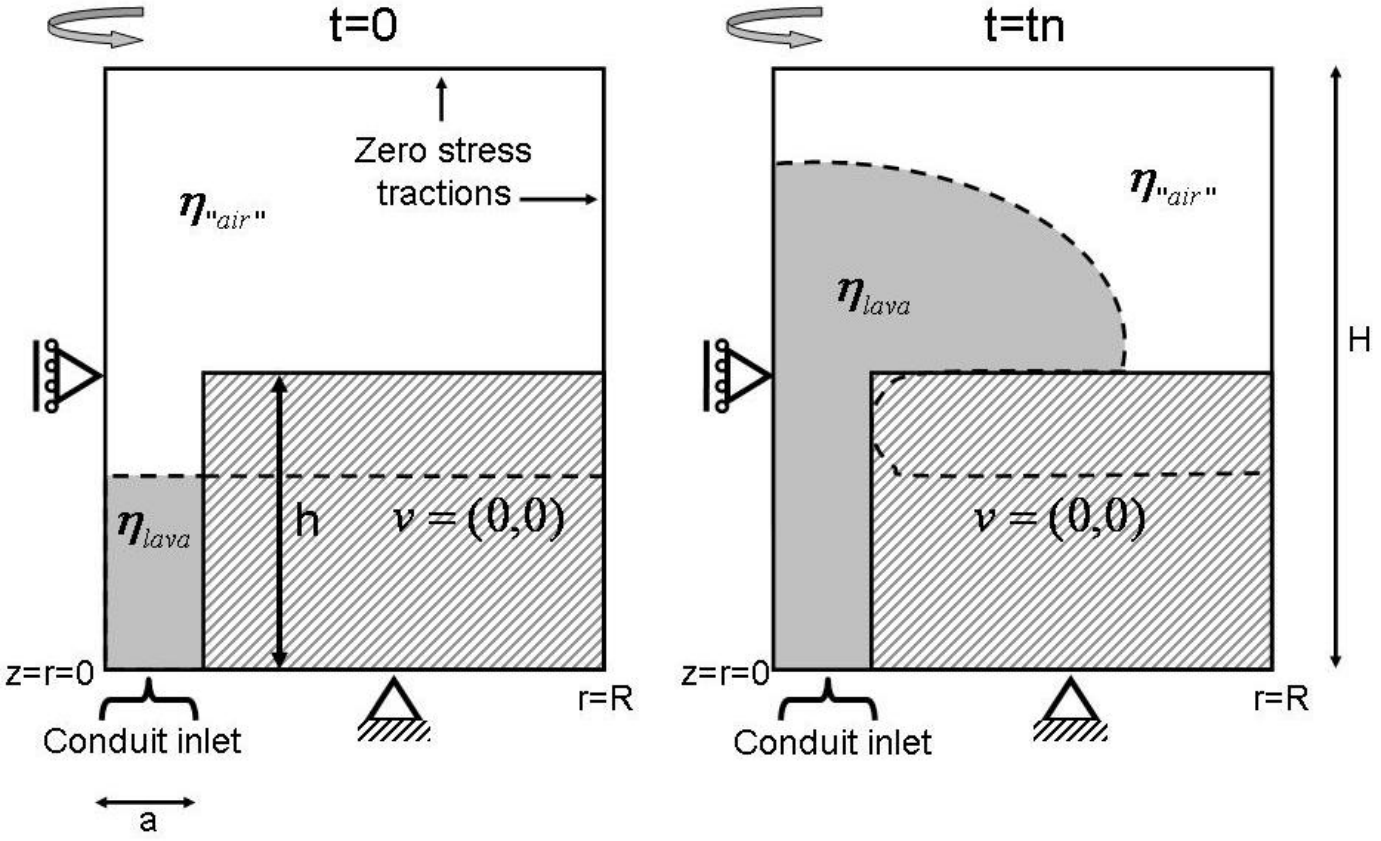

983
984
985 2

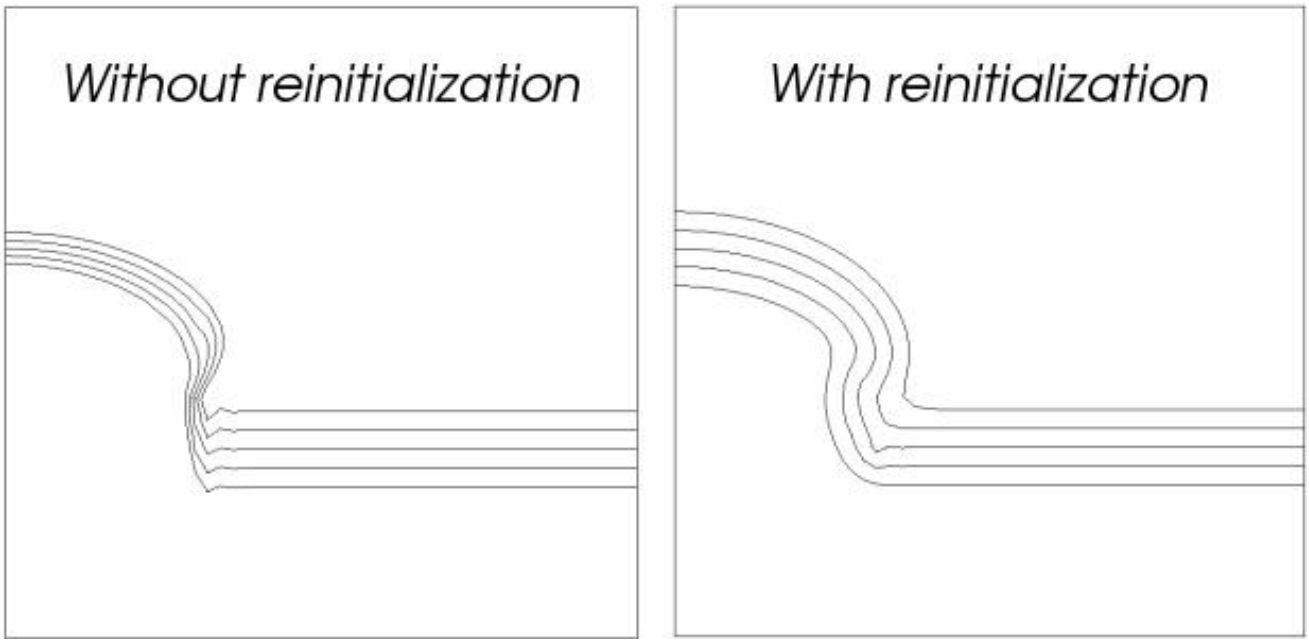

986
987

988 3

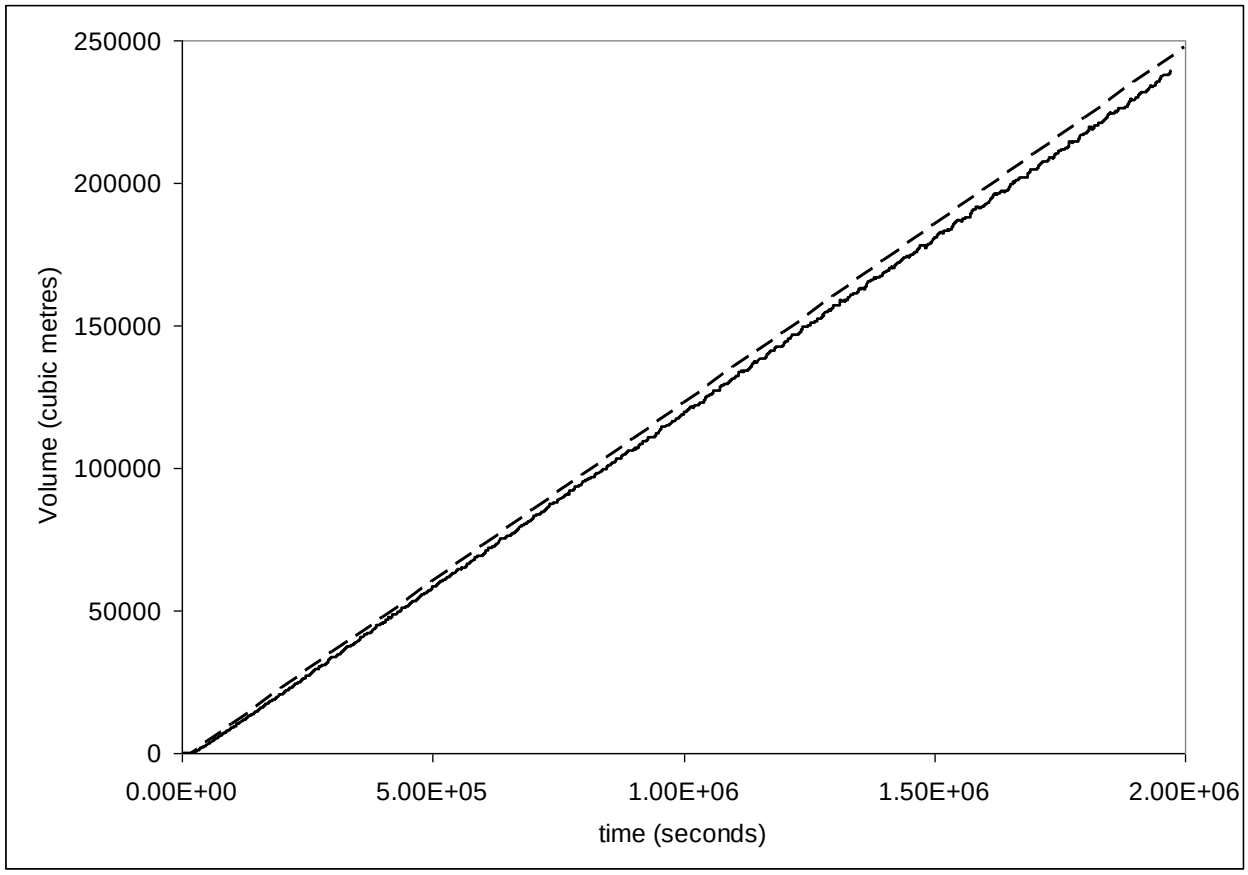

989
990
991
992 4

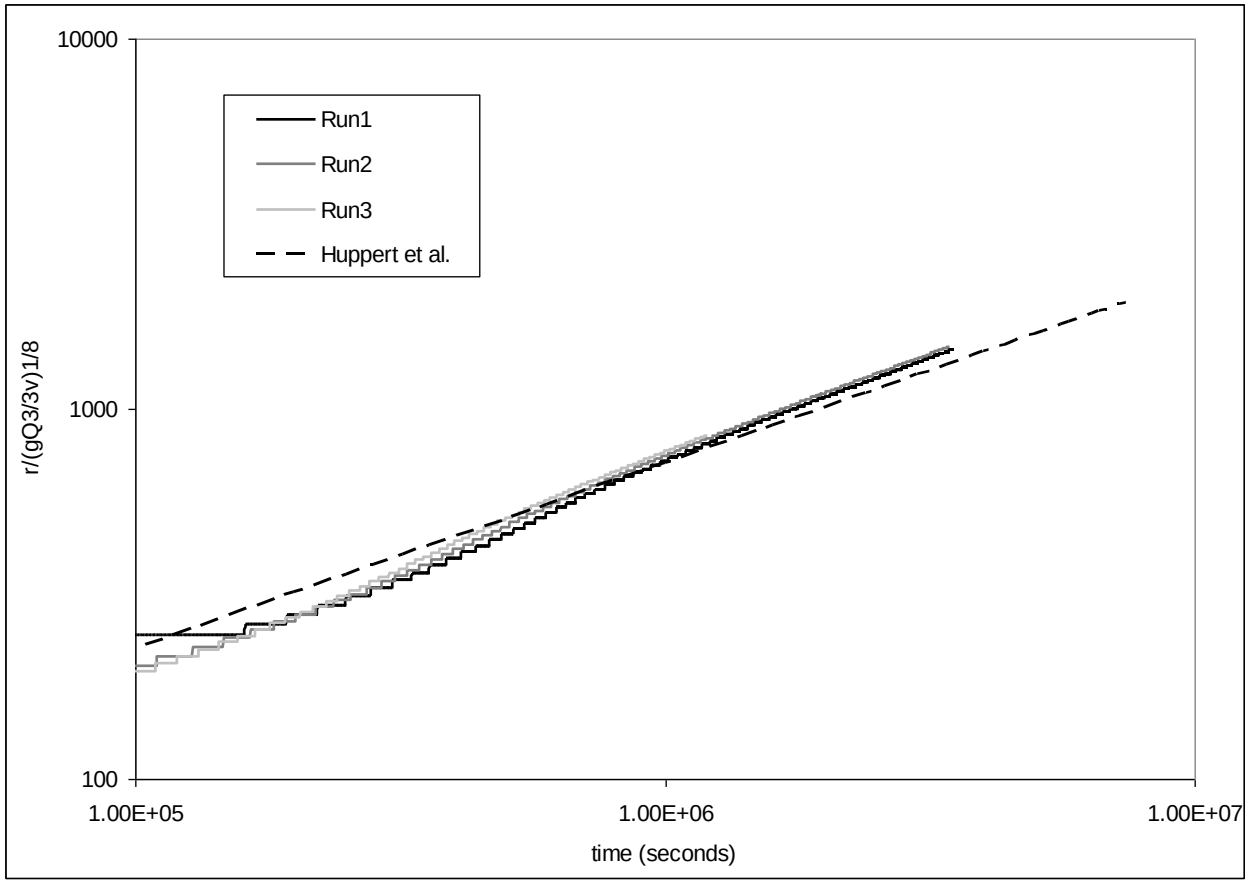
10000
1000
100
r/(gQ3/3v)1/8
Run1
Run2
Run3
Huppert et al.
1.00E+05
1.00E+06
1.00E+07
time (seconds)

5

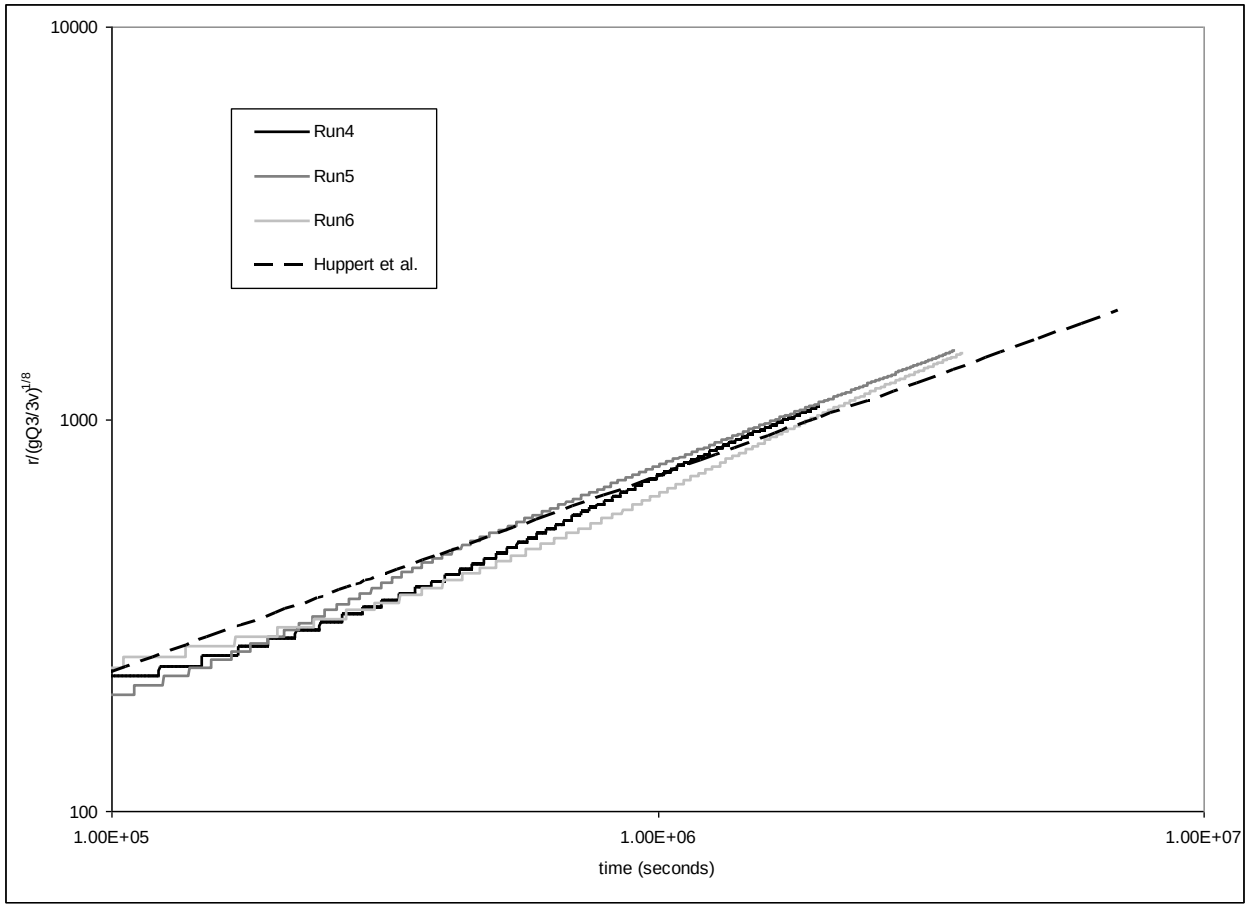
10000
1000
100
Run4
Run5
Run6
Huppert et al.
r/(gQ3/3ν)1/8
1.00E+05
1.00E+06
1.00E+07
time (seconds)

6

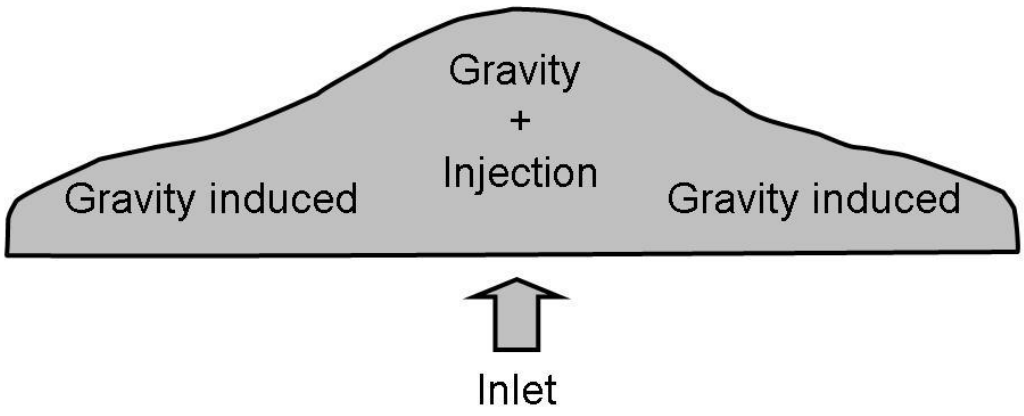
Gravity
+
Injection
Gravity induced
Gravity induced
Inlet

7a

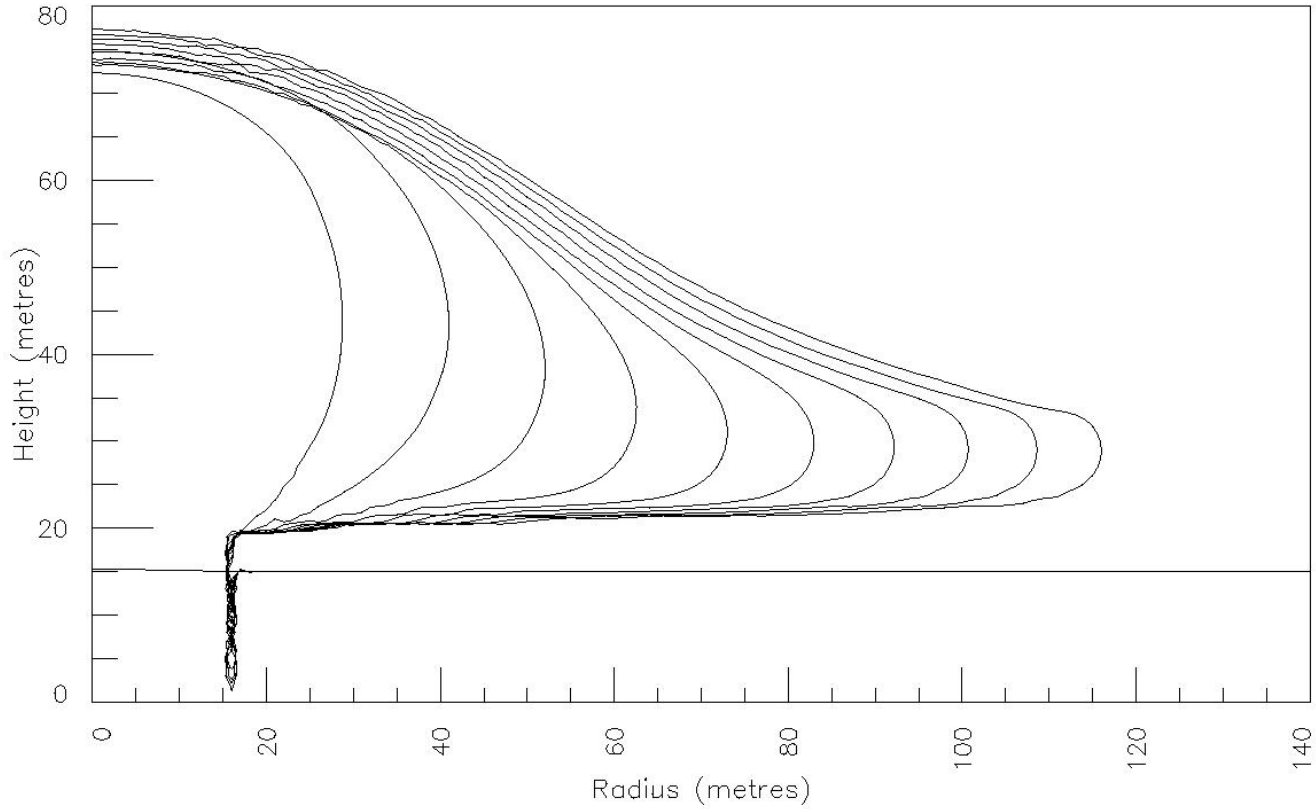

1002
1003 7b

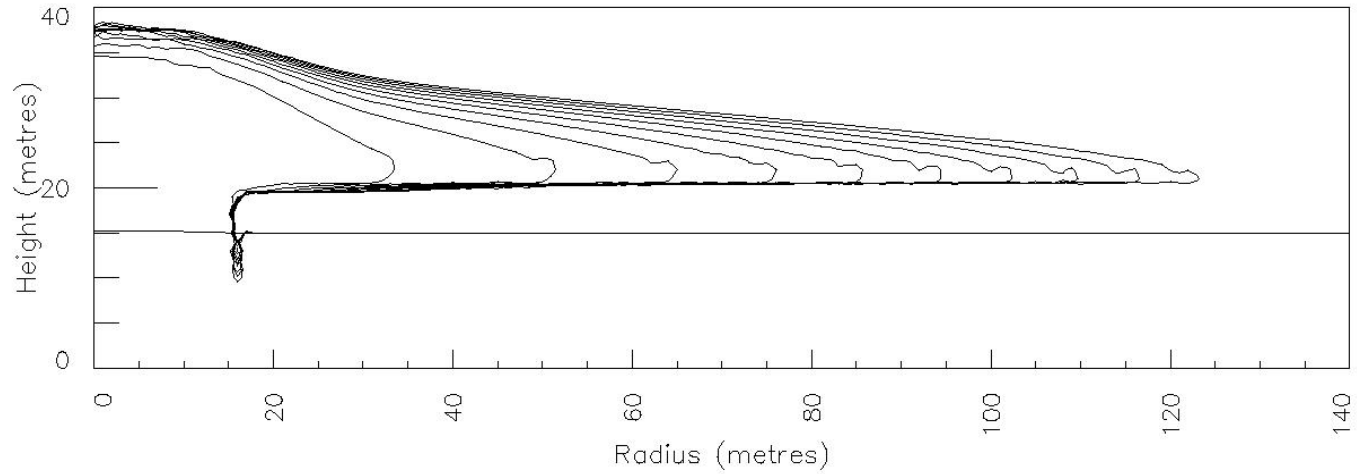

1004
1005

1006 8

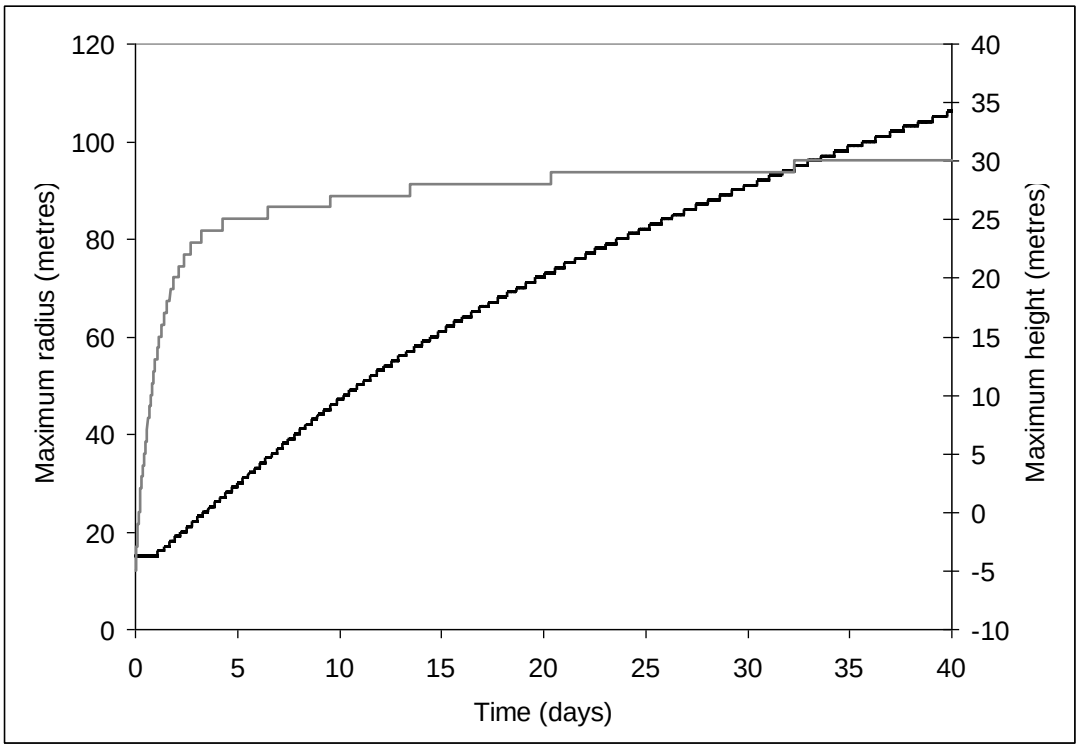

1007
1008
1009 9

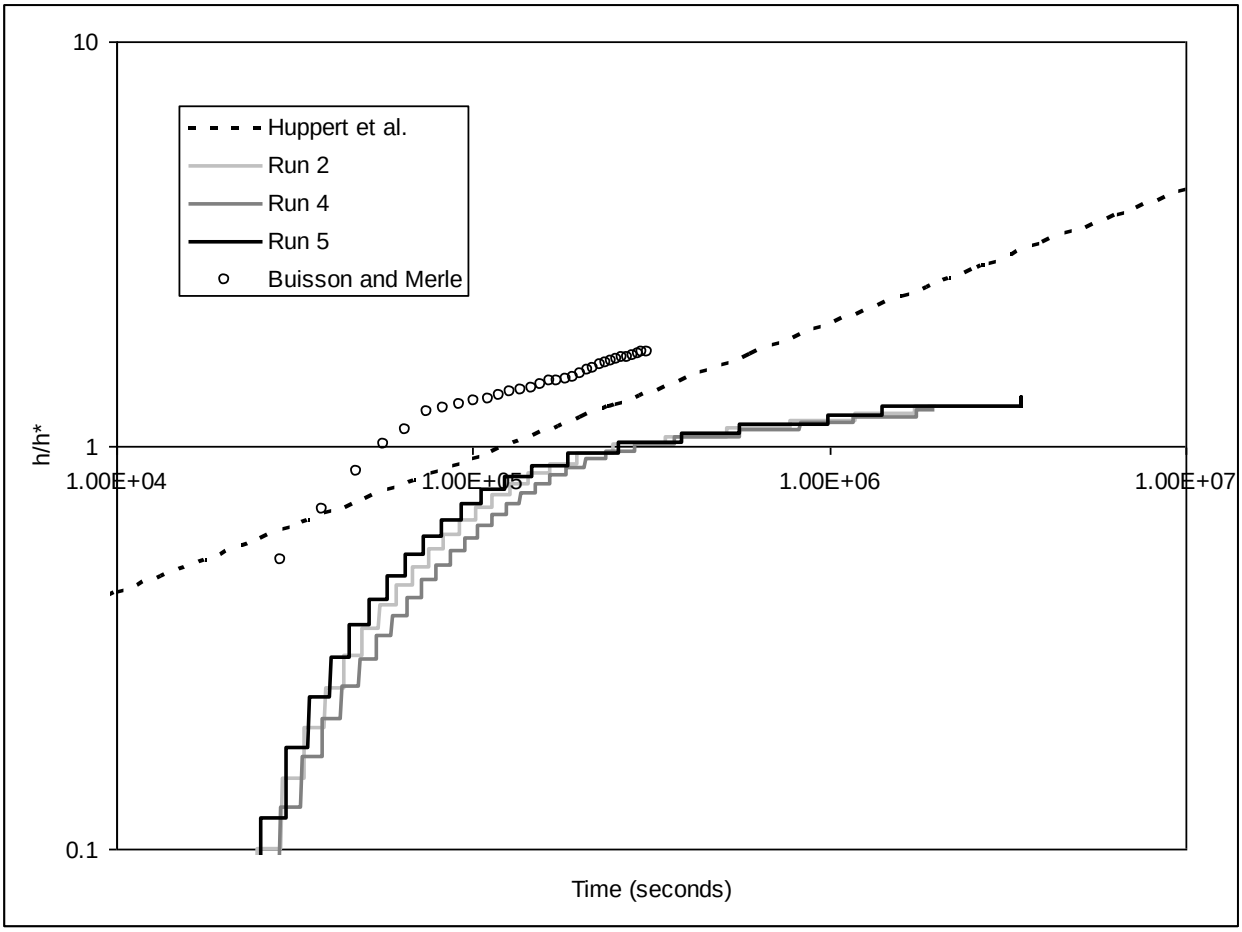

1010
1011
1012 10a to d

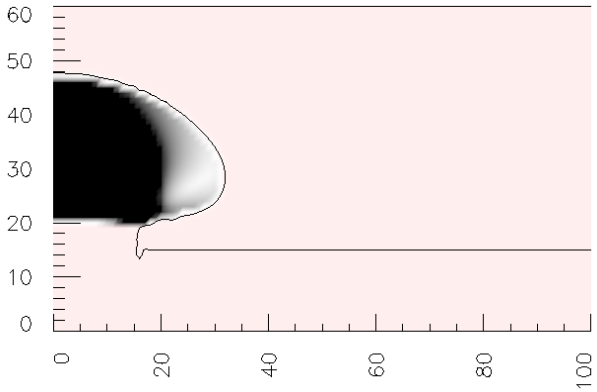

1013

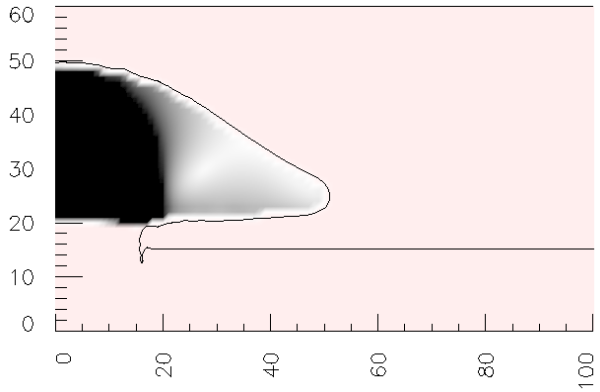

1014

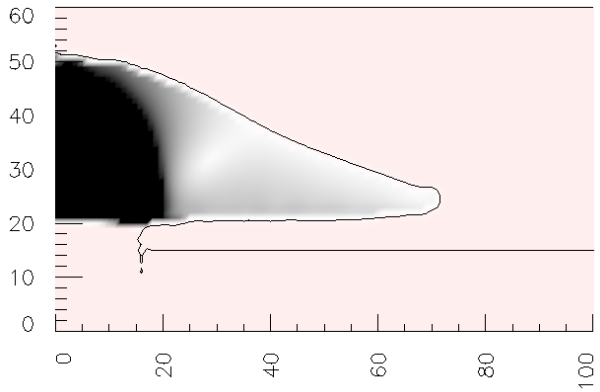

1015
1016

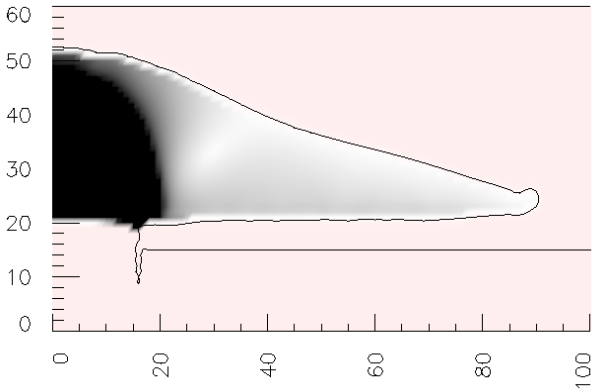

1017
1018 11

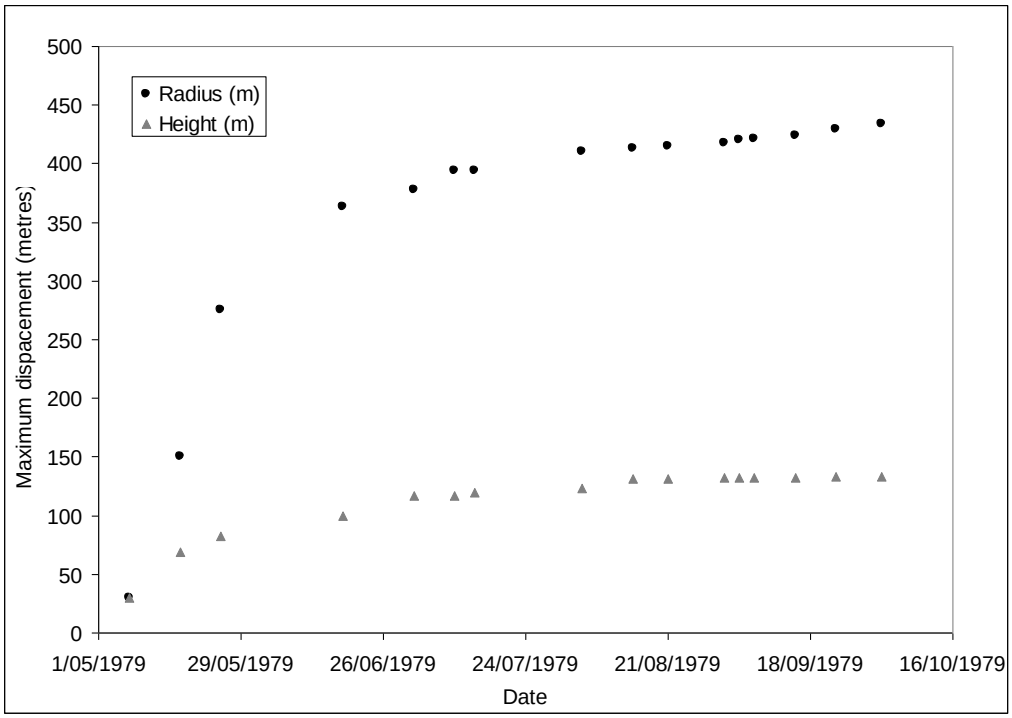

1019
1020
1021 12

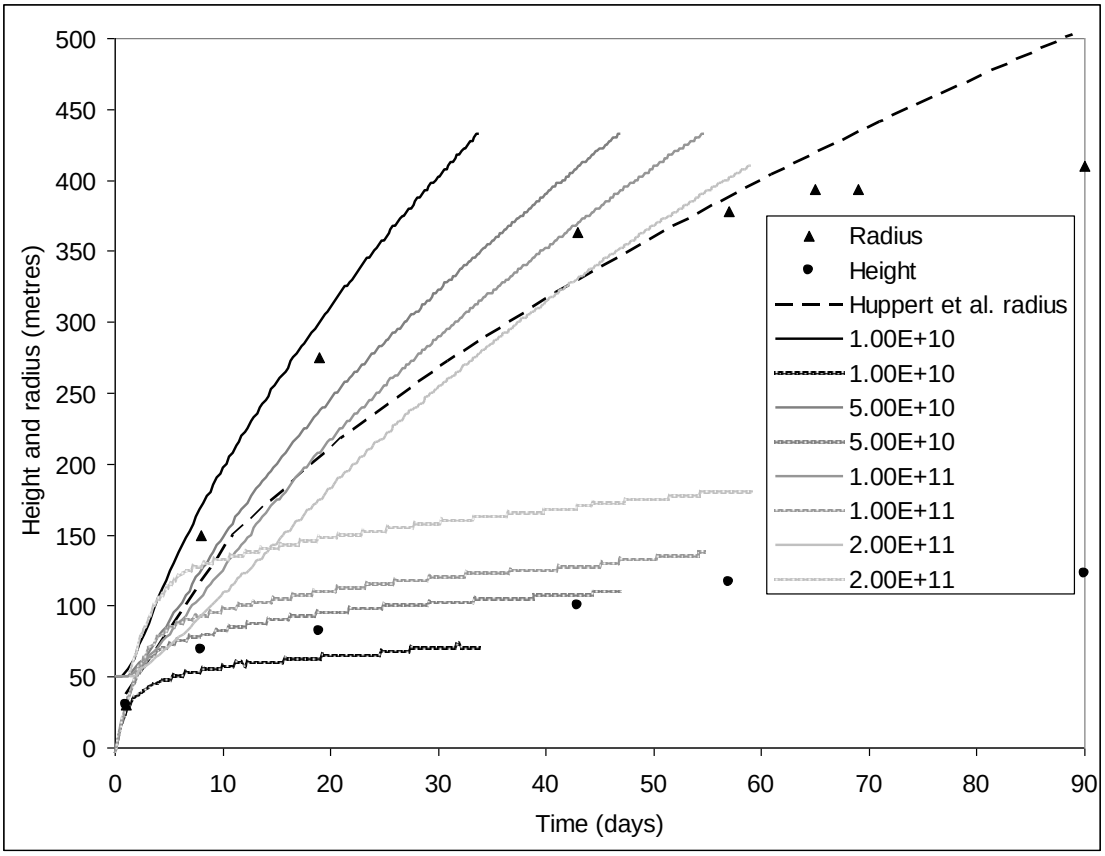

1022
1023 13

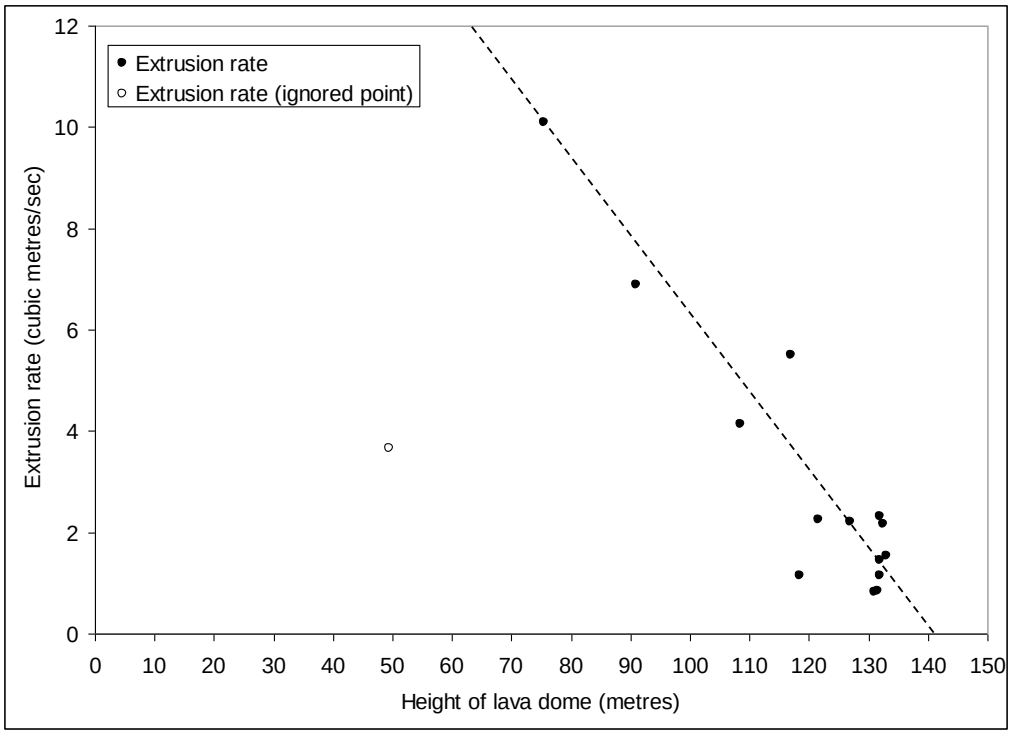
Extrusion rate
Extrusion rate (ignored point)
Extrusion rate (cubic metres/sec)
Height of lava dome (metres)
0
2
4
6
8
10
12
0
10
20
30
40
50
60
70
80
90
100
110
120
130
140
150

14

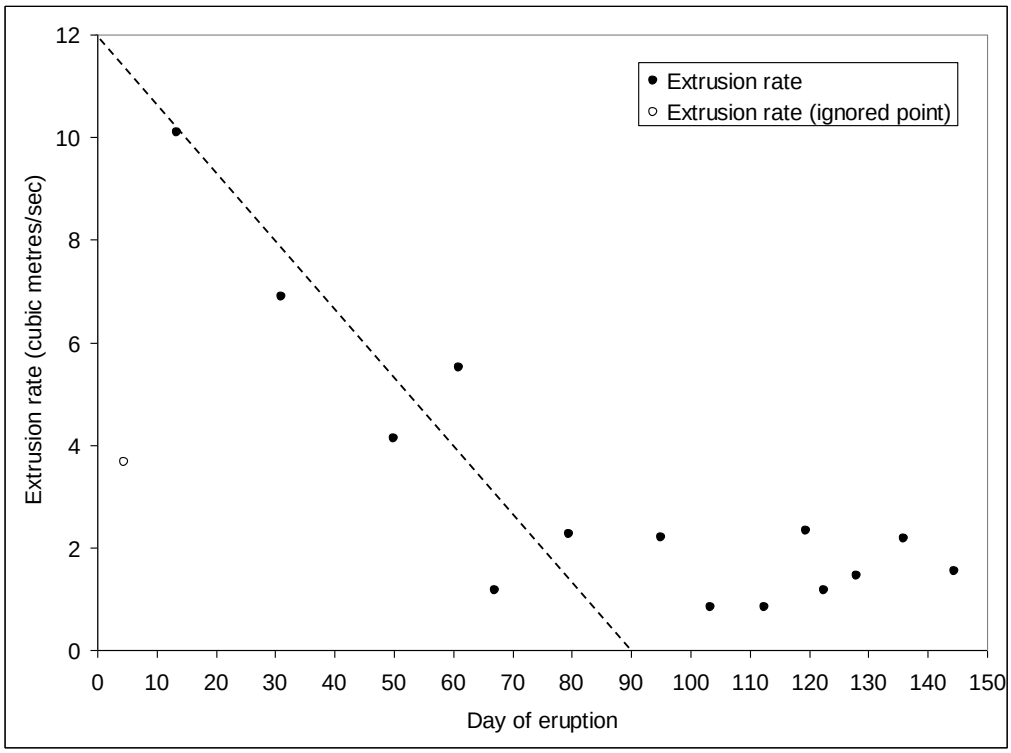
Extrusion rate
Extrusion rate (ignored point)
Extrusion rate (cubic metres/sec)
Day of eruption
0
2
4
6
8
10
12
0
10
20
30
40
50
60
70
80
90
100
110
120
130
140
150

15

1032

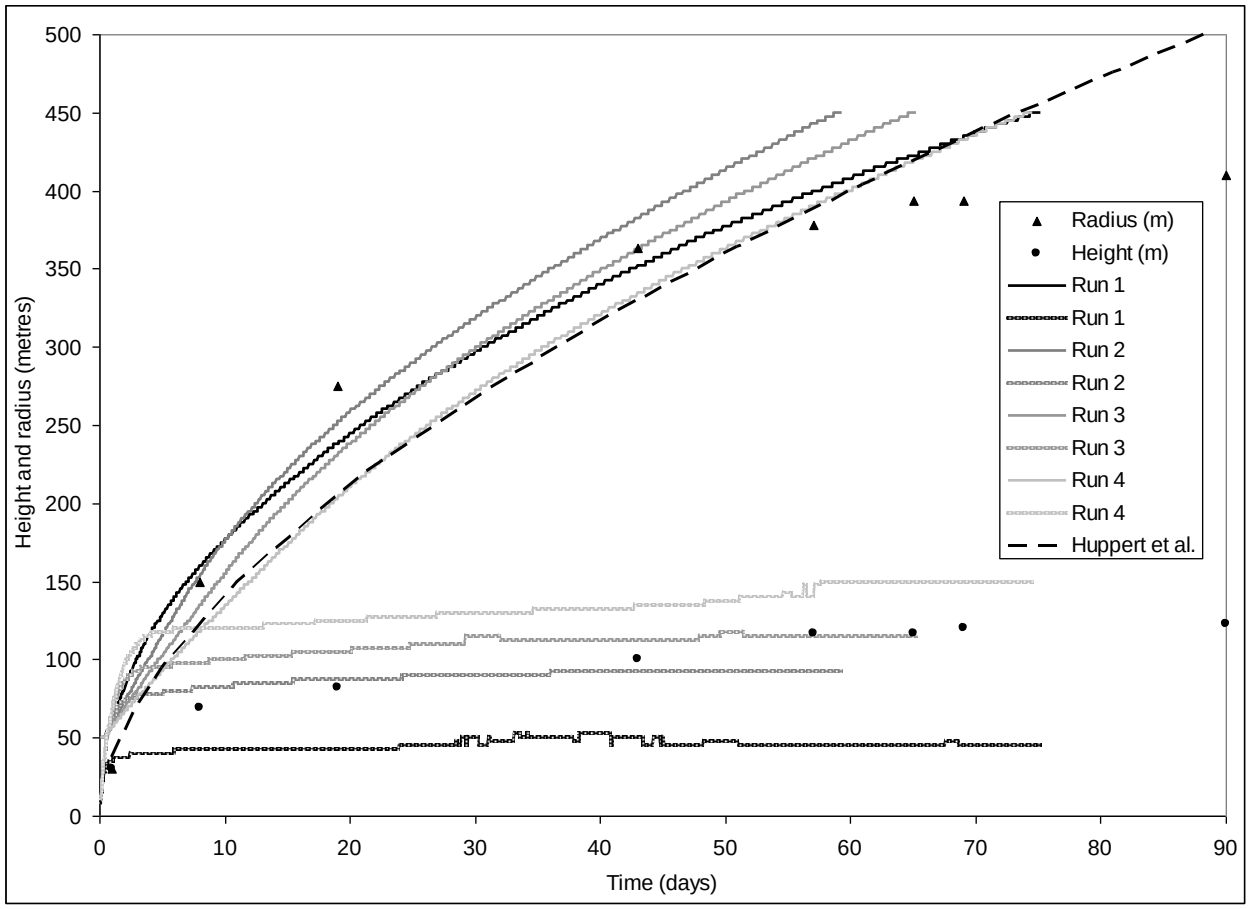

1033
1034
1035 16

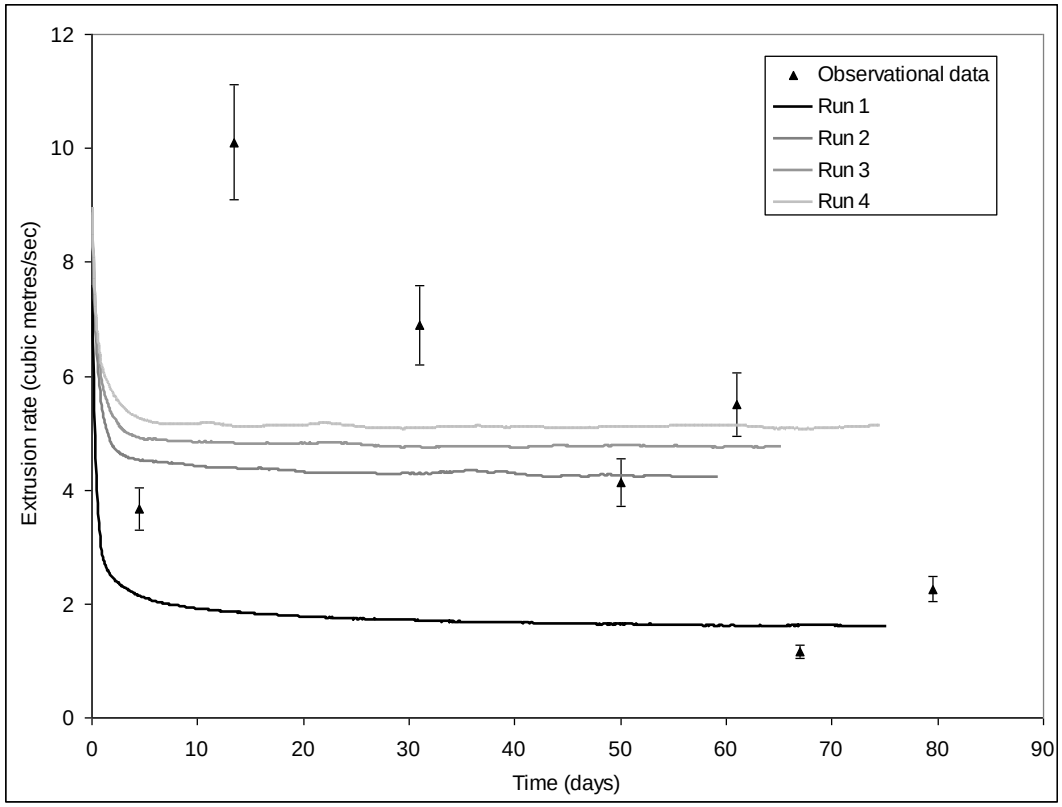
Observational data
Run 1
Run 2
Run 3
Run 4
Extrusion rate (cubic metres/sec)
Time (days)
0
2
4
6
8
10
12
0
10
20
30
40
50
60
70
80
90

17

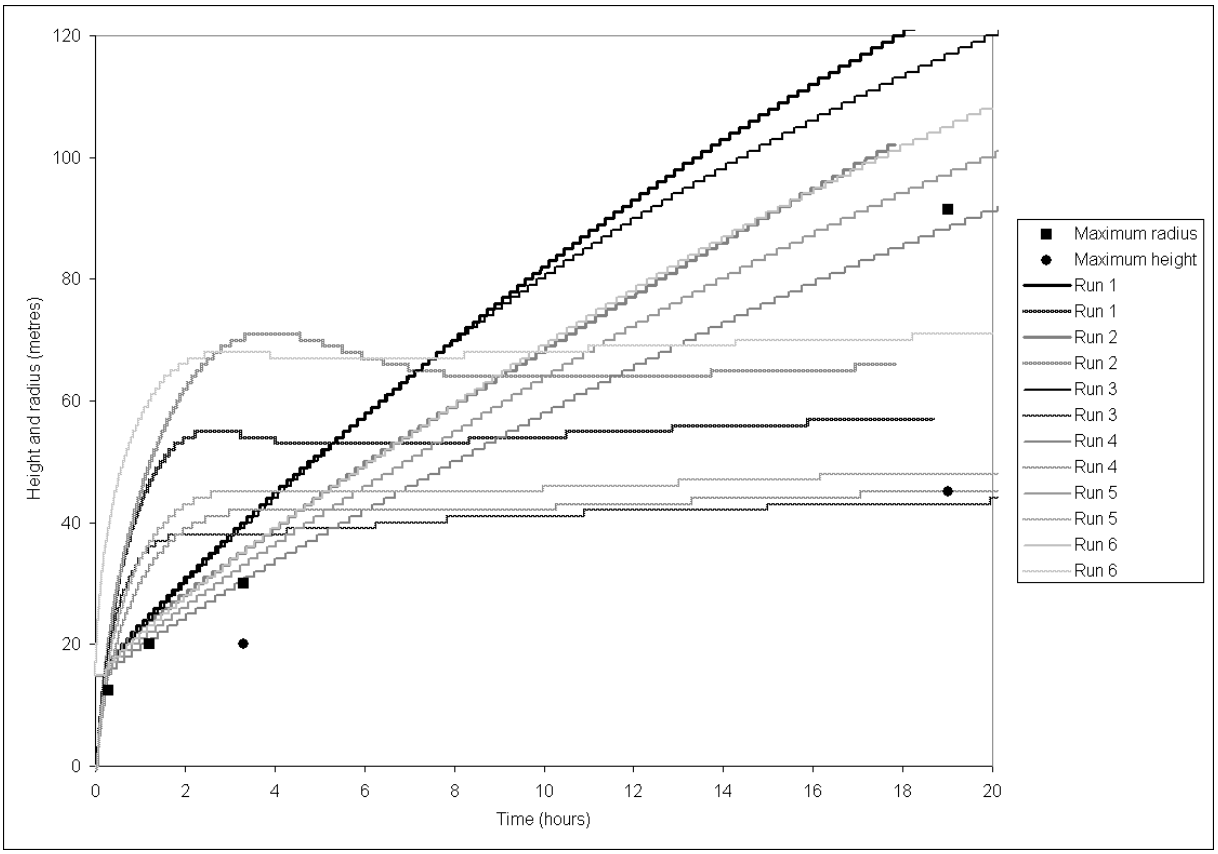
Maximum radius
Maximum height
Run 1
Run 1
Run 2
Run 2
Run 3
Run 3
Run 4
Run 4
Run 5
Run 5
Run 6
Run 6
Height and radius (metres)
Time (hours)
0
20
40
60
80
100
120
0
2
4
6
8
10
12
14
16
18
20

1039 18

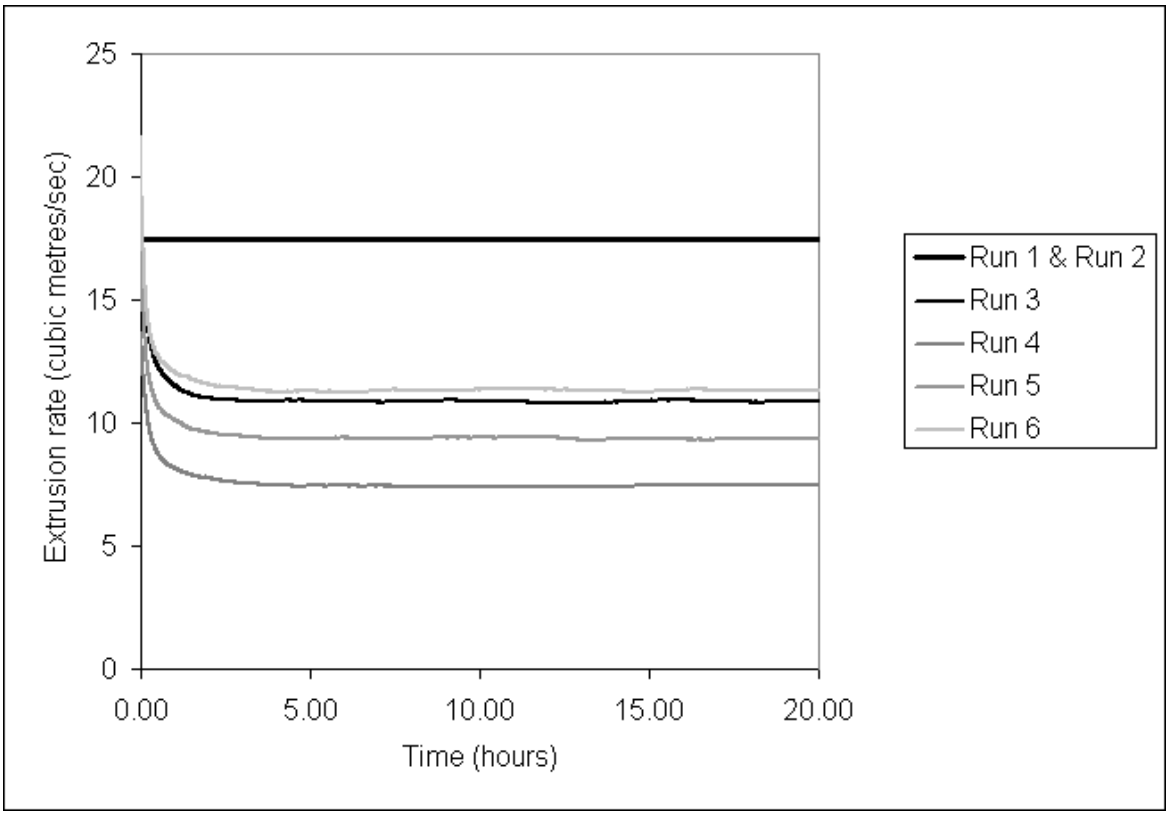
25
20
15
10
5
0
Extrusion rate (cubic metres/sec)
0.00
5.00
10.00
15.00
20.00
Time (hours)
Run 1 & Run 2
Run 3
Run 4
Run 5
Run 6

1040